Extended POLIPHON dust conversion factor dataset for lidarderived cloud condensation nuclei and ice-nucleating particle concentration profiles

Yun He^{1,2,3}, Goutam Choudhury⁴, Matthias Tesche⁵, Albert Ansmann⁶, Fan Yi^{1,2,3}, Detlef Müller⁷, and Zhenping Yin^{7,*}

¹School of Earth and Space Science and Technology, Wuhan University, Wuhan China

10

15

20

25

Abstract. Mineral dust is abundant in the atmosphere. To assess its climate impact, it is essential to obtain information on the three-dimensional distribution of cloud condensation nucleation (CCN) and ice-nucleating particle (INP) concentrations related to mineral dust. The POlarization LIdar PHOtometer Networking (POLIPHON) method uses aerosol-type-dependent conversion factors to transform lidar-derived aerosol optical parameters into CCN- and INP-relevant microphysical parameters. We present a global data set of conversion factors at 532 nm obtained using Aerosol RObotic NETwork (AERONET) observations at 137 sites for INP and 123 sites for CCN calculations. Dust presence is identified using a column-integrated dust ratio threshold of 80%, derived from AERONET columnar particle linear depolarization ratio at 1020 nm. INP-relevant conversion factors ($c_{250,d}$, $c_{s,d}$, and $c_{s,100,d}$) exhibit distinct regional patterns, generally lower near deserts and increasing downstream from dust sources. CCN-relevant conversion factors ($c_{100,d}$ and χ_d) display significant site-to-site variation. A comparison of dust-related particle concentration profiles derived using both POLIPHON and the independent OMCAM (Optical Modelling of the CALIPSO Aerosol Microphysics) retrieval shows that profiles generally agree within an order of magnitude. This result is consistent with the respective retrieval uncertainties and corroborates the usefulness of lidar observations for inferring dust-related CCN and INP concentration profiles.

²Key Laboratory of Geospace Environment and Geodesy, Ministry of Education, Wuhan, China.

³State Observatory for Atmospheric Remote Sensing, Wuhan, China.

⁴Department of Environment, Planning and Sustainability, Bar-Ilan University, Ramat Gan, Israel.

⁵Leipzig Institute for Meteorology (LIM), Leipzig University, Leipzig, Germany.

⁶Leibniz Institute for Tropospheric Research (TROPOS), Leipzig, Germany

⁷School of Remote Sensing and Information Engineering, Wuhan University, Wuhan, China.

^{*}Correspondence to: Zhenping Yin (zp.yin@whu.edu.cn)

1. Introduction

30

35

40

45

50

55

60

65

70

Aerosol-cloud interactions (ACI) contribute the largest uncertainty in our current understanding of global climate change (IPCC, 2021). To study ACIs, it is essential to link characteristic parameters of both aerosols and clouds. Parameters such as cloud phase, cloud fraction, ice/liquid water content, and the size and number concentrations of ice crystals and liquid droplets are typically used for estimating the climate effect of clouds (Huang et al., 2006; Rosenfeld et al., 2014). Estimates of the climate effect of aerosols are often based on aerosol optical depth (AOD), aerosol index, or aerosol number concentration (Nakajima et al., 2001; Rosenfeld, 2006; Zhao et al., 2019). A better assessment of ACI effects requires information on the number concentration of cloud-relevant aerosol particles at cloud level, particularly of ice nucleating particles (INP) and cloud condensation nuclei (CCN) (Kanji et al., 2017; Korolev et al., 2017).

The POLIPHON (POlarization LIdar PHOtometer Networking) method has been developed for inferring INP and CCN number concentration profiles from ground-based lidar measurements (Mamouri and Ansmann, 2014, 2015; Mamouri et al., 2016). It has also been applied to lidar observations from space (Marinou et al., 2019; Choudhury et al., 2022). This method combines polarization lidar observations with sun photometer measurements, meteorological parameters (from reanalysis or radiosonde data), and aerosol-type specific parameterizations to retrieve profiles of INP concentrations (INPC) and CCN concentrations (CCNC). Therefore, the POLIPHON method holds potential for global application, ranging from individual or multiple ground-based lidar sites (Ansmann et al., 2019a, 2019b; Haarig et al., 2019; Marinou et al., 2019; Hofer et al., 2020; He et al., 2021b) to spaceborne lidar observations, such as CALIOP (Cloud-Aerosol Lidar with Orthogonal Polarization) (Winker et al., 2009; Georgoulias et al., 2020; He et al., 2022; Shen et al., 2024) and ongoing EarthCARE mission (Wehr et al., 2023), and ground-based lidar networks (Baars et al., 2016; Pappalardo et al., 2014).

An essential step of POLIPHON is the transformation of lidar-derived aerosol-type-specific extinction coefficients to particle number concentrations (with particle size above a certain threshold) and particle surface area concentrations as input to INP- and CCN-parameterizations with the help of related conversion factors (Ansmann et al., 2019a; He et al., 2021b, 2023). However, for each aerosol type, conversion factors can vary from region to region due to differences in particle microphysics. The global application of POLIPHON therefore requires spatially resolved information about these conversion factors.

Dust aerosols are of particular importance as they mark a major contributor to global INP and CCN burden (Kanji et al., 2017; Choudhury and Tesche, 2022a; Casquero-Vera et al., 2023; Chatziparaschos et al., 2024; Herbert et al., 2025). The most challenging aspect of deriving dust-related conversion factors is identifying the presence of dust in sun photometer observations, such as in the framework of the Aerosol Robotic Network (AERONET, Holben et al., 1998; Giles et al., 2023). So far, POLIPHON studies have used an Ångström exponent (AE, for 440–870 nm) <0.3 and AOD at 532 nm >0.1 (Ansmann, et al., 2019a) or a column-integrated dust ratio >53% (based on the 1020-nm particle linear depolarization ratio) (He et al., 2023) for identifying dust-dominated observations. Here we aim to extend the earlier work on dust-related conversion factors to additional AERONET sites that cover most regions on Earth where local or transported dust aerosols are likely to occur.

The extended conversion-factor dataset can be applied to retrieving dust-related CCNC and INPC profiles that can be compared to independent datasets or measurements. The uncertainties in POLIPHON-derived INPC are primarily caused by the considered INP parameterizations (DeMott et al., 2015; Ullrich et al., 2017). Those are highly dependent on meteorological parameters, which makes INPC comparison a very challenging task. In contrast, CCN parameterizations are much simpler (Shinozuka et al., 2015) and easily applicable in a validation study. Therefore, we will compare dust-related CCNC profiles derived from spaceborne CALIOP observations using POLIPHON with those obtained by the Optical Modelling of the CALIPSO Aerosol Microphysics (OMCAM, Choudhury and Tesche, 2022a, 2022b, 2023a) retrieval. OMCAM assumes that each aerosol type can be represented by a single particle size distribution (PSD). This fundamental difference to POLIPHON provides us with a unique opportunity to examine the potential influence (sensitivity to retrieving uncertainty) of such an assumption in CCNC retrievals.

The paper is organized as follows. We first introduce the POLIPHON method, the process for retrieving dust-related

conversion factors, and the OMCAM algorithm. Section 3 presents the derived dataset of dust-related conversion factors. In Section 4, we conduct a dust-related CCN profile comparison study between the POLIPHON and OMCAM methods. The main findings of the study are summarized in Section 5.

2. Data and methodology

75

80

85

90

95

2.1 POLIPHON method for dust-related CCN and INP retrieval

POLIPHON was developed for deriving height-resolved aerosol-type-specific information on particle mass, INPC, and CCNC based on measurements with polarization lidar and sun photometer (Mamouri and Ansmann, 2014, 2015; Mamouri et al., 2016). The method is considered particularly reliable in the presence of mineral dust (Hofer et al., 2020; Ansmann et al., 2021b; He et al., 2021b) due to the large particle linear depolarization ratio of non-spherical dust particles (Tesche et al., 2009).

Table 1. Overview of the computation of dust-related mass, INP, and CCN concentrations using the POLIPHON method based on polarization lidar observations (Tesche et al., 2010; Ansmann et al., 2019a). The subscripts 'p', 'd', and 'nd' denote 'particle', 'dust', and 'non-dust', respectively.

Main task	Input parameter	Calculation	Uncertainties
Divide lidar-derived particle backscatter β into dust β_d	$\beta(z), \delta_{\mathrm{p}}(z)$	$\beta_{\rm d}(z) = \beta(z) \frac{\left(\delta_{\rm p}(z) - \delta_{\rm nd}\right)(1 + \delta_{\rm d})}{\left(\delta_{\rm d} - \delta_{\rm nd}\right)(1 + \delta_{\rm p}(z))}$	10-20%
and non-dust $eta_{ m nd}$	$\beta_{\rm d}(z)$, dust lidar ratio	$\alpha_{\rm d}(z) = LR \cdot \beta_{\rm d}(z)$	15-25%
Convert into dust mass	$\alpha_{\rm d}(z)$, dust-	$M_{\rm d}(z) = c_{\rm v,d} \times \rho_{\rm d} \times \alpha_{\rm d}(z)$	20-30%
concentration, CCN- and INP-relevant parameters: dust number concentration $n_{250,d}$ and $n_{100,d}$, and dust	related conversion factors	$n_{250,d}(z) = c_{250,d} \times \alpha_{d}(z)$	25-35%
		$s_{\rm d}(z) = c_{\rm s,d} \times \alpha_{\rm d}(z)$	30-40%
		$s_{100,d}(z) = c_{s,100,d} \times \alpha_{d}(z)$	20-30%
particle surface area concentration s_d and $s_{100,d}$		$\log(n_{100,d}(z)) = \log(c_{100,d}) + \chi_d \log(\alpha_d(z))$	50-200%
Input parameters $n_{250,d}$, s_d , $s_{100,d}$, and $n_{100,d}$ into different INP and CCN parameterizations	$n_{250,d}(z), T(z)$	INP parameterization D-15 (DeMott et al., 2015)	50-300%
	$s_{\rm d}(z), T(z)$	INP parameterization U-17d (Ulrich et al., 2017)	50-300%
	$s_{100,d}(z), T(z)$	INP parameterization U-17d (Ulrich et al., 2017)	50-300%
•	$n_{100, d}(z)$	CCN parameterization: $n_{\text{CCN,d}}(z) = f_{\text{ss,d}} \times n_{100,d}(z)$ (Shinozuka et al., 2015)	50-200%

The processing steps of POLIPHON are summarized in Table 1. The method starts with the retrieval of the particle backscatter coefficient β_p from lidar observations using the method of Fernald (1984). This parameter is separated into contributions from dust and non-dust, i.e., β_d and β_{nd} (Tesche et al., 2009). Next, the dust extinction coefficient α_d is obtained by multiplying β_d with a dust lidar ratio (LR) of 30-60 sr (Müller et al., 2007; Tesche et al., 2011; Hofer et al., 2017; Hu et al., 2020; Peng et al., 2021; Floutsi et al., 2023). Dust particles originating from different deserts can exhibit distinct optical and microphysical properties, such as particle size distribution and complex refractive index; additionally, variations in dust transport pathways may lead to differences in aging, mixing, and removal processes. These factors may result in regional-variation of the dust lidar ratio. The derived α_d is then converted into

- the concentration of particles with radii larger than 100 nm $(n_{100.d})$ for the CCN retrieval,
- the concentration of particles with radii larger than 250 nm $(n_{250,d})$ for the INP retrieval, and
- the surface area concentration s_d and $s_{100,d}$ for the INP retrieval

with the help of the corresponding conversion factors, i.e., $c_{100,d}$, χ_d , $c_{250,d}$, $c_{s,d}$, and $c_{s,100,d}$ (Mamouri et al., 2016; Ansmann et al., 2019a). It should be noted that, for retrieving the CCN-relevant parameter $n_{100,d}$, a log-log regression analysis is applied, in which the conversion factor $c_{100,d}$ and regression coefficient χ_d are determined (Shinozuka et al., 2015). Finally, $n_{250,d}$, s_d ,

and $s_{100,d}$ are used as input for various dust INP parameterization schemes (DeMott et al., 2015; Ulrich et al., 2017) to derive the dust-related INP profile $n_{\text{INP,d}}(z)$. $n_{100,d}$ is used to obtain the dust-related CCN profile $n_{\text{CCN,d}}(z)$ following Shinozuka et al. (2015) as:

$$n_{\text{CCN,d}}(z) = f_{\text{ss,d}} \times n_{100,d}(z) \tag{1}$$

where $f_{\rm ss,d}$ is the water supersaturation-dependent factor, with values of 1.00, 1.35, and 1.70 for supersaturations of 0.15-0.20%, 0.25%, and 0.40%, respectively. Note that for retrieving CCN and INP, $n_{\rm 250,d}$, $s_{\rm d}$, and $n_{\rm 100,d}$ under dry conditions are needed. Here dust is considered hydrophobic so an additional correction is not necessary (Mamouri et al., 2016).

In addition, from the dust extinction coefficient, we can also derive the dust mass concentration profile $M_d(z)$ by using the extinction-to-volume conversion factor $c_{v,d}$ and an assumed dust density ρ_d with the following equation (Jing et al., 2024):

$$M_{\rm d}(z) = \rho_{\rm d} \times \alpha_{\rm d}(z) \times c_{\rm v,d} \tag{2}$$

We assume ρ_d to be 2.6 g cm⁻³ (Ansmann et al., 2019a). The parameters $c_{v,d}$ and ρ_d together determine the so-called mass extinction efficiency (Wang et al., 2021). Detailed computational procedures, associated equations, and uncertainty analyses are provided in Mamouri and Ansmann (2015) and Ansmann et al. (2019a).

2.2 Conversion factors derived from AERONET dataset

100

105

110

115

120

125

130

135

The conversion factors in the POLIPHON method are dependent on both aerosol type and geographic region (Ansmann et al., 2019a). In this section, we describe the retrieval of $c_{v,d}$, $c_{100,d}$, χ_d , $c_{250,d}$, and $c_{s,d}$. To ensure consistency with Ansmann et al. (2019a), we also present the conversion factor $c_{s,100,d}$ for calculating the surface area concentration of dust particles with radii larger than 100 nm. These conversion factors are derived from AERONET measurements of AOD at eight wavelengths (i.e., 340, 380, 440, 500, 675, 870, 1020, and 1064 nm) (Holben et al., 1998; Giles et al., 2019) and the particle size distributions provided in the aerosol inversion data product (Sinyuk et al., 2020) as illustrated in Figure 1. The first step is identifying the presence of dust in an observation. We use the columnar particle linear depolarization ratio (PLDR) at 1020 nm δ_{1020nm}^p from the AERONET inversion product for identifying dust data points (Noh et al., 2017; Shin et al., 2018, 2019; He et al., 2023). Due to the spheroid particle assumption in the AERONET algorithm, PLDR at the near-infrared wavelength may show some overestimations as compared with polarization lidar observations (Toledano et al., 2019; Haarig et al., 2022). Nevertheless, its polarization sensitivity is sufficient for identifying nonspherical particles. Dust is the primary nonspherical particle in the atmosphere; thus, we consider other potential types of nonspherical aerosols, such as fresh smoke, volcanic ash, and pollen as secondary.

We calculate the column-integrated dust ratio $R_{\rm d,1020nm}$ following Shin et al. (2019):

$$R_{\rm d,1020nm} = \frac{\left(\delta_{\rm 1020nm}^{\rm p} - \delta_{\rm nd}^{\rm p}\right)\left(1 + \delta_{\rm d}^{\rm p}\right)}{\left(\delta_{\rm d}^{\rm p} - \delta_{\rm nd}^{\rm p}\right)\left(1 + \delta_{\rm 1020nm}^{\rm p}\right)} \tag{3}$$

where the dust $\delta_{\rm d}^{\rm p}$ and non-dust $\delta_{\rm nd}^{\rm p}$ PLDR values are set to 0.30 and 0.02, respectively. Within the atmospheric column, $R_{\rm d,1020nm}$ reflects the contribution of dust to the total particle backscatter coefficient of an external aerosol mixture (Tesche et al., 2009). For reference, lidar observations of the PLDR of pure dust range between 0.30 and 0.35 (Freudenthaler et al., 2009; Floutsi et al., 2023). In this extended study, we use $R_{\rm d,1020nm} \geq 80\%$ as a criterion for identifying the 'dust-presence' data points, which are subsequently used to calculate the conversion factors for dust aerosols. We have conducted a sensitivity analysis by adjusting this threshold value for the column-integrated dust ratio that we used to identify dust-containing data points. Varying this criterion largely affects the number of AERONET sites for which conversion factors are available. The selection of an optimal threshold involves balancing data availability and closeness to pure dust conditions. The use of $R_{\rm d,1020nm} \geq 80\%$ marks a compromise between the identification of pure dust cases with $0.89 < R_{\rm d,1020nm} \leq 1$, which potentially may be too strict, and the inclusion of a large amount of non-dust aerosols for dust-dominated mixtures with $0.53 \leq R_{\rm d,1020nm} < 0.89$.

For each identified data-presence data point (from number j = 1 to J_d , where J_d is the number of identified dust-containing data points), we can obtain the dust-related conversion factors ($c_{v,d}$, $c_{250,d}$, $c_{s,d}$ and $c_{s,100,d}$) using the particle size distribution and AOD data, following equations (6) and (9)-(11) in Ansmann et al. (2019a). The 532-nm AOD is converted from 500-nm AOD by using the Ångström exponent between 440 and 870 nm, respectively. To retrieve $c_{100,d}$ and χ_d , we apply the regression analysis below (also given in Table 1):

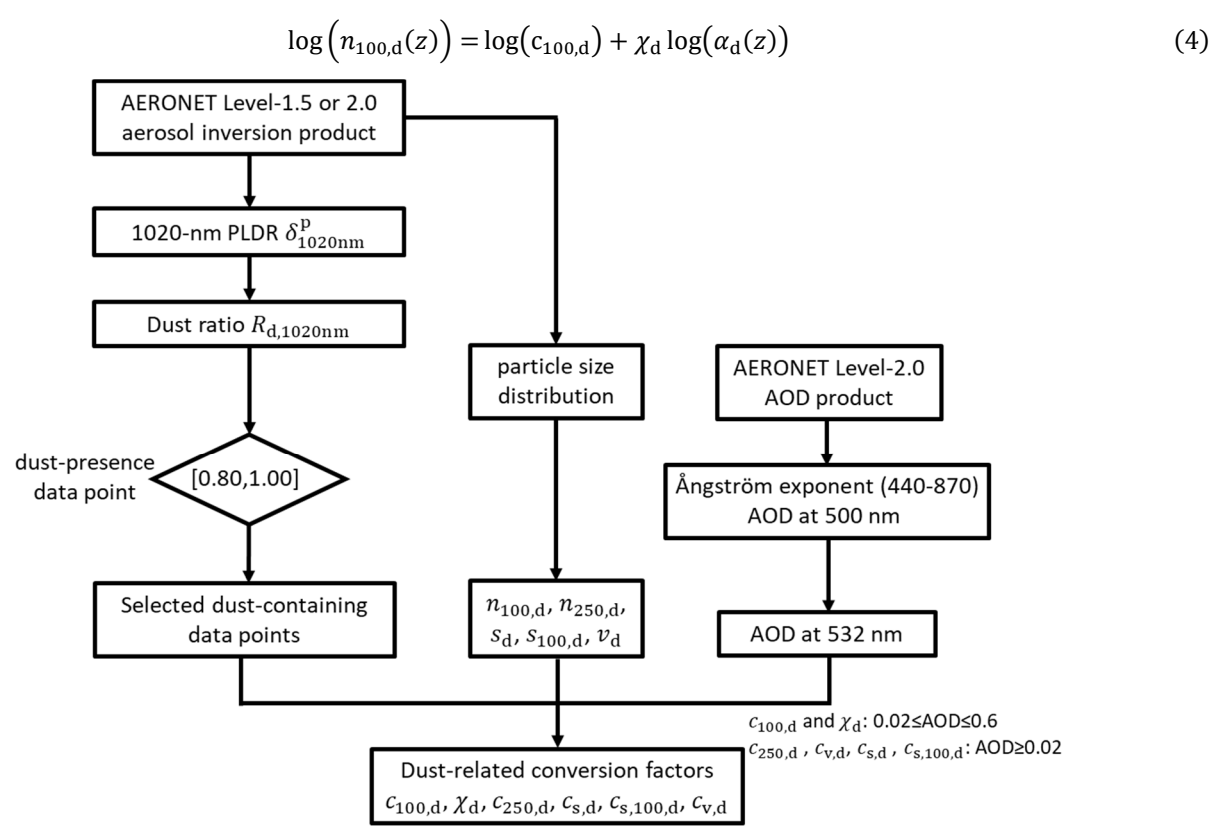


Figure 1. Flow chart of calculating the dust-related POLIPHON conversion factors based on the AERONET measurements, including the Version 3 Level-1.5 or -2.0 aerosol inversion product (corresponding to the finally obtained Level-1.5 or -2.0 conversion factor dataset, respectively) (Sinyuk et al., 2020; AERONET, 2023b) and Level-2.0 AOD product (Giles et al., 2019; AERONET, 2022a). The selection scheme of dust-containing data points refers to Shin et al. (2018, 2019).

Figure 2 shows the AERONET sites selected for retrieving the dust-related conversion factors in this study. We only include AERONET sites with valid data spanning observations of more than two years before October 2022 (AERONET, 2023a, 2023b). In total, 198 AERONET sites are included, geographically covering most desert regions and the major transport pathways of dust plumes (Hu et al., 2019; Mona et al., 2023). The origin of dust particles at each site can be quite variable. In the tropic and mid-latitude of the Northern Hemisphere, a majority of dust particles generally appears along the dust belt that spans the Saharan Desert, Middle East deserts, Asian deserts (mainly the Taklimakan Desert and Gobi Desert), and their downstream regions (Hofer et al., 2017). The high-latitude dust of the Northern Hemisphere can be contributed by high-latitude local Aeolian dust origins (Bullard et al., 2016) as well as south-to-north meridional transport originating from Asian and African deserts (Shi et al., 2022). In the Southern Hemisphere, there are major dust sources including the Patagonian Desert in South America, Australia's deserts, and the Kalahari Desert in Southern Africa. In addition, anthropogenic dust from agriculture, transportation, or construction, can also play a significant role (Chen et al., 2023).

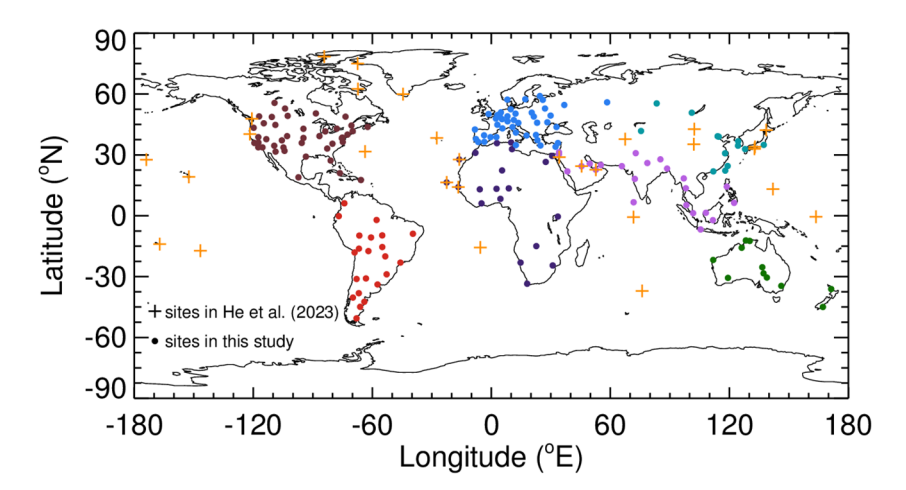


Figure 2. Overview of AERONET sites used for inferring dust-related POLIPHON conversion factors. The orange crosses show the locations of near-desert, oceanic, and coastal sites in He et al. (2023). The solid circles in different colors indicate the locations of 198 AERONET sites in North America (dark red), South America (red), Africa (modena), Europe (blue), North and East Asia (lilac), South and West Asia (magenta), and Australia (green).

2.3 OMCAM algorithm for retrieving CCN concentration

165

170

175

180

185

190

Choudhury and Tesche (2022a) developed the OMCAM algorithm to derive global, height-resolved aerosol-type-specific CCNC from spaceborne CALIPSO (Winker et al., 2009) lidar observations. To calculate dust-related CCNC, they obtain dust-related backscatter and extinction coefficients from three aerosol mixtures in the CALIOP level-2 aerosol profile product, namely mineral dust, polluted dust, and dusty marine, following Tesche et al. (2009). The CALIPSO aerosol model provides microphysical properties of each aerosol type included in the retrieval (Omar et al., 2009). It provides a dust-specific normalized volume size distribution ($V_{\rm d,normalized}$) and refractive index which is used to obtain the corresponding dust extinction coefficient at 532 nm ($\alpha_{\rm d,normalized}$), through light-scattering calculations (Gasteiger and Wiegner, 2018). The ratio $V_{\rm t}$ of the CALIOP-measured dust extinction $\alpha_{\rm d,measured}$ and $\alpha_{\rm d,normalized}$ is used to scale the normalized volume size distribution to obtain:

$$V_{\rm d,scaled} = V_{\rm t} \times V_{\rm d,normalized} \tag{5}$$

This scaled size distribution $V_{d,scaled}$ is the one that best reproduces the dust extinction coefficient provided in the CALIPSO aerosol profile product. Converting $V_{d,scaled}$ into a number size distribution and using Eq. (1) leads to the dust-related CCNC profiles.

The instantaneous and gridded OMCAM-derived CCNC are found to be consistent with independent in-situ measurements (Choudhury and Tesche, 2022b; Choudhury et al., 2022; Aravindhavel et al., 2023) and reanalysis results (Choudhury et al., 2025). They are also used for studying aerosol-cloud interactions for warm and cold clouds based on spaceborne observations (Alexandri et al., 2024). Choudhury and Tesche (2023a) applied the OMCAM algorithm to generate the first global 3-D CCNC dataset using more than 15 years of CALIOP Level-2 aerosol profile products. This CCNC dataset includes five aerosol subtypes, i.e., marine, dust, polluted continental, clean continental, and elevated smoke. It is available at a uniform latitude-longitude grid of 2°×5° with a temporal resolution of one month.

2.4 Scheme of comparing dust CCNC from POLIPHON and OMCAM

There are several algorithms for retrieving CCNC profiles from lidar observations that all hinge on the assumed parameters of the PSD. Those methods are generally based on multiwavelength lidar data and might consult look-up tables (Lv et al., 2018; Zhou et al., 2024), in-situ measurements (Tan et al., 2019), or machine learning (Redeman and Gao, 2024) to convert optical data to microphysical parameters and offer the advantage of considering realistic and variable PSD estimates (Müller et al., 2014). However, the instrumental complexity required to obtain the data used in the abovementioned methods has so far

ruled out spaceborne application.

195

200

205

210

215

220

OMCAM has been designed for retrieving aerosol-type-specific CCNC from spaceborne lidar observations. POLIPHON has initially been developed for retrieving aerosol-type-specific CCNC and INPC based on ground-based lidar observations, and has subsequently been extended to spaceborne applications (Marinou et al., 2019). Therefore, a key difference between the OMCAM and POLIPHON methods is that OMCAM only employs a fixed shape of aerosol-type-specific PSD from CALIPSO's aerosol model, whereas POLIPHON considers the use of regionally varying aerosol-type-specific PSDs (i.e., conversion factors that are calculated from PSDs). In particular, regional variations in dust PSD mainly result from the deposition of dust particles during their long-range transport (Ansmann et al., 2017; Rittmeister et al., 2017). Coarse dust particles generally deposit prior to fine dust particles within the plume along the transport pathway from their dust sources (Ratcliffe et al., 2024), which causes variations in dust PSD. By comparing dust CCNC results obtained from these two methods, this study also provides an opportunity to evaluate whether employing a fixed dust PSD is sufficient for deriving the global dust CCNC distribution or whether regionally dependent dust PSDs are necessary (Adebiyi et al., 2023).

In this study, the monthly dust-related CCNC profiles obtained via POLIPHON and from the OMCAM climatology (Choudhury and Tesche, 2023b) are compared for selected AERONET sites. For consistency, both methods consider monthly dust-specific extinction coefficient profiles from the CALIOP Level 2 profile product for inferring CCNC in grid boxes closest to the considered AERONET stations. First, the CALIOP Version 4.20 Level-2 aerosol profile product (Omar et al., 2009) undergoes several data quality control procedures, as listed in Section 3.1.1 of Choudhury and Tesche (2023a). Next, we separate dust backscatter coefficient profiles from the aerosol subtypes of dust, polluted dust, and dusty marine using the method of Tesche et al. (2009). These dust backscatter coefficient profiles, combined with an assumed dust lidar ratio of 44 sr (Kim et al., 2018), are then used to form a global gridded (latitude: 2°, longitude: 5°) monthly-average dust extinction coefficient dataset, with a vertical resolution of 60 m from the surface to an altitude of 8 km. This 3-D global dust extinction dataset, derived from the CALIOP data spanning June 2006 to December 2021 (except for February 2016 due to the unavailability of CALIOP data), serves as inputs for retrieving dust-related CCNC implementing with both the POLIPHON and OMCAM methods.

3. Global distribution of dust-related conversion factors

Figure 3 presents dust-related conversion factors at four (out of 198) typical city sites, i.e., Beijing (China), KAUST_Campus (Saudi Arabia), La_Parguera (Puerto Rico), and Granada (Spain). Note that we use the formal site names defined by AERONET. The large difference in the number of dust-presence data points is due to both the duration of sun photometer observations and the frequency and extent of dust intrusions. The local atmospheric environment varies from site to site, as indicated by the averaged 532-nm AODs of 0.438, 0.374, 0.130, and 0.132 for Beijing, KAUST_Campus, La_Parguera, and Granada, respectively. Beijing shows larger $c_{v,d}$ and smaller $c_{250,d}$ compared to the other sites, which is probably due to the influence of more local pollutants (usually smaller size with larger concentration). This is discussed further below.

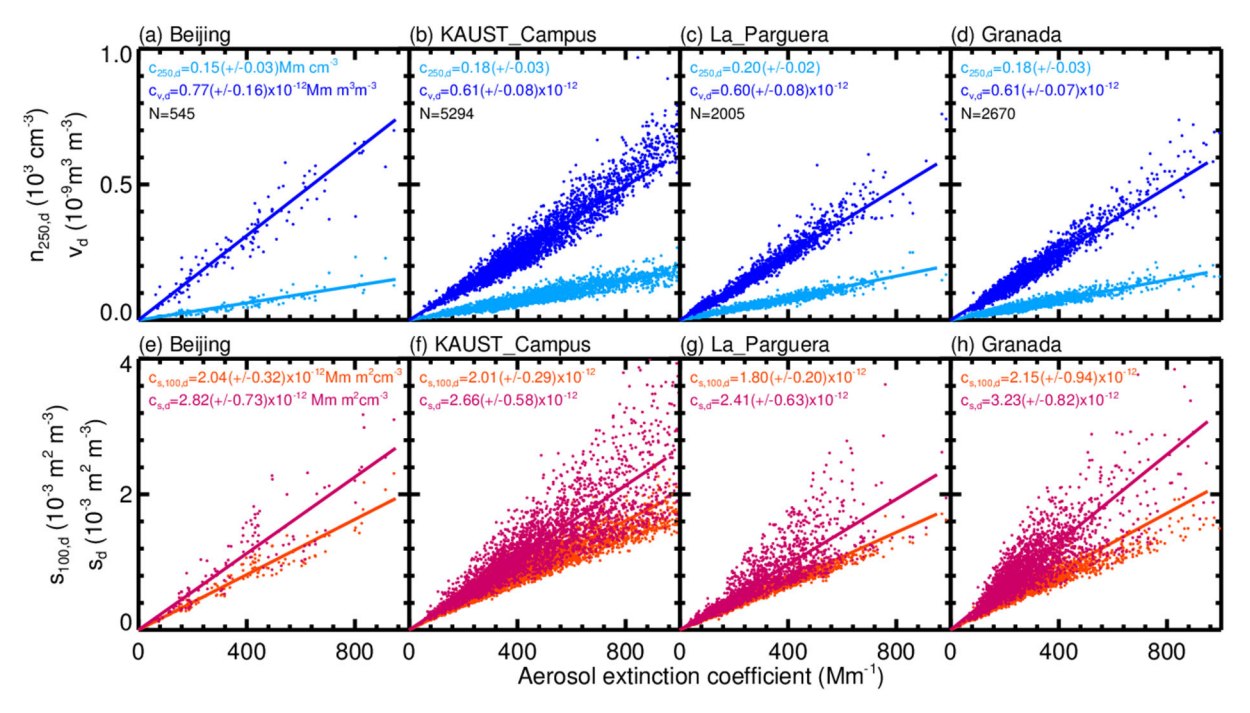


Figure 3. Relationship between the 532-nm aerosol extinction coefficient and particle (radius >250 nm) number concentration $n_{250,d}$, volume concentration v_d , and surface area concentration s_d and $s_{100,d}$ (radius >100 nm) for dust-presence data points (number denoted by N) at four typical city sites, i.e., (a) and (e) for Beijing (39.98°N, 116.38°E), (b) and (f) for KAUST_Campus (22.30°N, 39.10°E), (c) and (g) for La_Parguera (17.97°N, 67.05°W), and (d) and (h) for Granada (37.16°N, 3.61°W). The corresponding dust-related conversion factors are provided in the corresponding panels.

Figure 4 presents the global distribution of dust-related mass concentration and INP-relevant conversion factors $c_{v,d}$, $c_{250,d}$, $c_{s,d}$ and $c_{s,100,d}$. Ansmann et al. (2019) applied a threshold value of AOD>0.1 (i.e., aerosol extinction >100 Mm⁻¹) when calculating INP- and CCN-related dust conversion factors, and thereby excluded cases with very clean atmospheric conditions that may introduce large uncertainties in the computations. He et al. (2023) attempted to relax this lower limit to an AOD of 0.02 (i.e., aerosol extinction >20 Mm⁻¹) to increase the number of available data points and eliminate abnormal values. Based on the comparisons with Ansmann et al. (2019), we find that loosening relaxing this threshold value does not significantly affect the results. Therefore, we only considered data points with aerosol extinctions exceeding 20 Mm⁻¹. For a site to be considered, it had to show at least 15 valid dust-presence data points, which applies to 137 out of the 198 selected AERONET sites. The regional variation of the conversion factors reflects the distinct microphysical properties of dust along its transport pathways and the varying impact of mixing with other aerosol types (Philip et al., 2017). Moreover, dust from different deserts may exhibit different microphysical properties. Particularly changes in the dust PSD contribute to the regional variation of conversion factors.

As shown in Figure 4a, the extinction-to-volume conversion factor $c_{v,d}$ ranges from 0.4×10^{-12} to 0.8×10^{-12} Mm·m³·m³ over the dust belt region of the Northern Hemisphere (e.g., North Africa, the Middle East, and Central Asia) as well as the major downstream regions of dust transport (Europe, East Asia, and Western America). In addition, similar $c_{v,d}$ values are also obtained in some Australian sites impacted by local desert dust. Values of $c_{v,d}$ generally decrease along the routes of dust transport due to the removal of dust particles by gravitation settling and cloud processing as well as the mixing with other, usually smaller and more spherical aerosols. This is consistent with the dust-related conversion factors found at Lanzhou near the deserts in East Asia and Wuhan far away from deserts (He et al., 2021b). Kai et al. (2023) observed a decreasing trend in the dust mass-extinction conversion factor along the transport pathway of dust aerosols originating from the Gobi Desert, which suggests an equivalent decreasing trend in $c_{v,d}$, if assuming a fixed dust density. The larger geographical coverage of

the data set presented here provides valuable information for global dust models in which mass extinction efficiency is a key parameter (Adebiyi et al., 2020; Han et al., 2022). In contrast, Figure 4b shows that $c_{250,d}$ near desert regions are relatively lower compared to polluted regions downstream of deserts. Notably, a gradual increase in $c_{250,d}$ is evident when following the meridional transport of dust from North Africa to Northern Europe, corresponding to the typical northward transport pathway of Saharan dust. Generally, $c_{s,d}$ and $c_{s,100,d}$ show slightly higher values at the sites far from desert regions. Moreover, these two factors are more sensitive to the presence of other aerosols (He et al., 2023), which may explain the larger site-to-site variation.

255

260

265

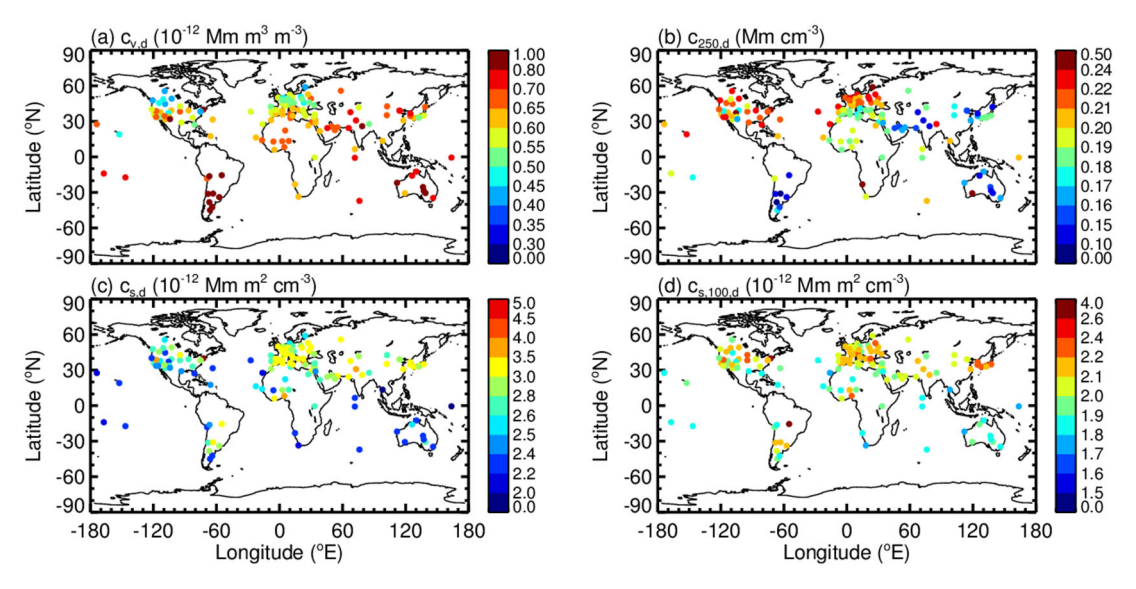


Figure 4. POLIPHON dust-related conversion factors $c_{v,d}$, $c_{250,d}$, $c_{s,d}$ and $c_{s,100,d}$ obtained from dust data points ($R_{d,1020nm} \ge 80\%$) at 137 AERONET sites.

Figure 5 shows the derived CCN-relevant conversion factors $c_{100,d}$ and χ_d at four typical city sites, i.e., the same as those in Figure 3. Note that only data points with aerosol extinctions between 20 Mm⁻¹ and 600 Mm⁻¹ are considered in the calculations. The correlations at Beijing, Granada, and La_Parguera are generally strong; however, at KAUST_Campus, the data points tend to be scattered as the aerosol extinction coefficient increases, indicating a growing influence of local non-dust particles, e.g. anthropogenic pollutants.

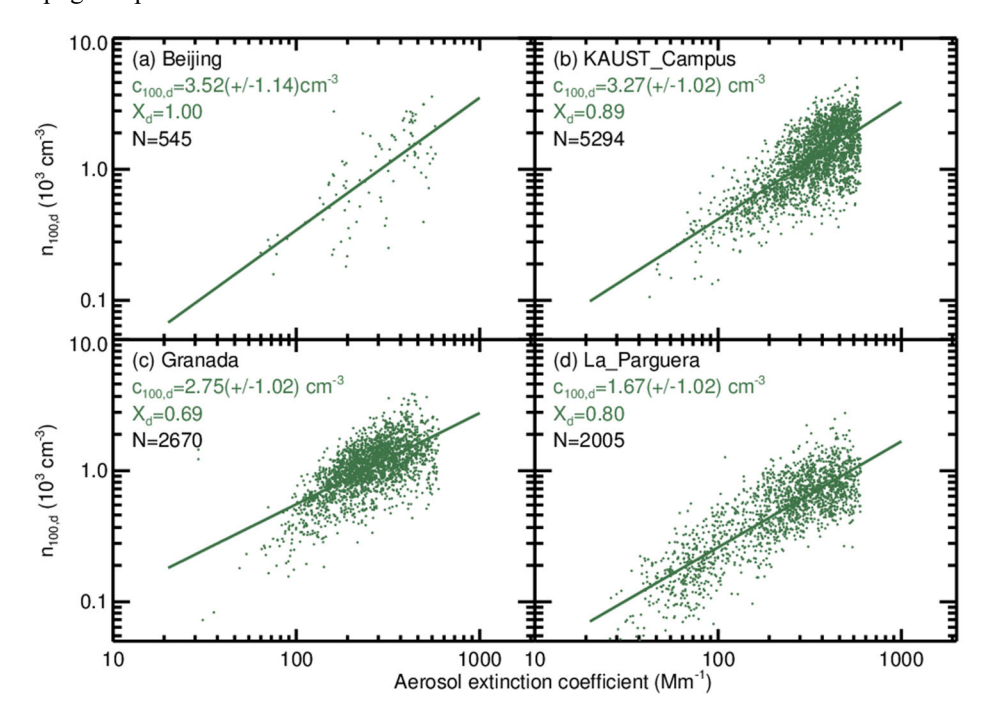


Figure 5. Relationship between aerosol extinction coefficient at 532 nm and aerosol particle number concentration $n_{100,d}$ (radius >100 nm) for dust-presence data points at the same sites as Figure 3. The corresponding dust-related conversion factors $c_{100,d}$ and χ_d are provided.

270

275

280

285

290

295

300

Figure 6 presents the distribution of worldwide $c_{100,d}$ and χ_d values. When applying the regression analysis, Ansmann et al. (2019a) found that the relationship becomes much weaker when the 532-nm AOD exceeds 0.6 (i.e., extinction coefficient >600 Mm⁻¹); the authors provide a thorough discussion on this issue (see Section 3.2 therein). Accordingly, we allocated extinction coefficients between 20 Mm⁻¹ to 600 Mm⁻¹ to the identified dust-containing data points and calculated the CCN-related conversion factors. For each site, the conversion factors are considered only if at least 15 valid dust-presence data points are available. As a result, 123 out of the 198 selected AERONET sites have valid conversion factors. No identifiable regional variation pattern is observed for $c_{100,d}$ and χ_d , indicating that these factors are more sensitive to the contribution of local fine-mode particles. This suggests that to derive dust-related CCNC, it is crucial to use region-specific conversion factors rather than relying on a global average, which is consistent with the results given by Ansmann et al. (2019a).

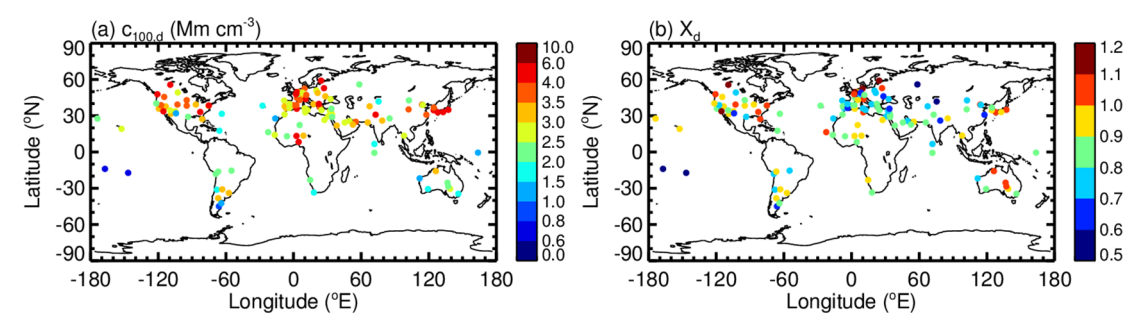


Figure 6. POLIPHON dust-related conversion factor $c_{100,d}$ and associated regression coefficient χ_d obtained from dust data points $(R_{d,1020nm} \ge 80\%)$ at 123 AERONET sites.

The conversion factors presented in Figures 4 and 6 can be accessed at https://doi.org/10.5281/zenodo.16781089 (He, 2025). Note that a conversion factor is provided only when the corresponding number of identified dust-presence data points exceeds 15. Considering the use of dust-dominant mixture (with a columnar dust ratio $R_{d,1020nm} \ge 80\%$) in the calculation, traces of local non-dust components (e.g., anthropogenic pollutants) may be included. Therefore, a larger dust-presence data point number and a smaller standard deviation indicate that the corresponding conversion factors more closely represent the local dust properties. Note that the results from the dust belt region of the Northern Hemisphere are considered more reliable (Hofer et al., 2017), as they typically involve over 1000 dust-presence data points. In contrast, the results from downwind sites located in more remote regions of dust transport, such as North and South America, likely reflect occasional dust intrusion events (long-range transport), meaning that the derived conversion factors may not be representative from a statistical point of view, and thus, we recommend further validations by in-situ measurements. We have also endeavored to compile a gridded dust conversion-factor dataset for expedient future use in studying global ACI using gridded spaceborne lidar datasets. However, this has proven challenging due to the limited number of available sites in comparison to global coverage and their inhomogeneous geographical distribution. Therefore, when applying this conversion factor dataset, we recommend selecting values from the nearest available site.

4. Comparing dust-related CCN concentrations from POLIPHON and OMCAM

We verify the extended conversion-factor dataset by comparing the obtained dust-related CCNC profiles with OMCAMderived CCN data (Choudhury and Tesche, 2022a, 2023a) for 12 AERONET sites. The sites were selected to provide a wide geographical spread and to cover the range of χ_d from 0.7 to 1.1. Table 2 gives an overview of those sites and the inferred parameters. More details can be found in the dataset (He, 2025). The CCNC values from geographical grids containing the selected AERONET sites are extracted for comparison. It should be noted that dust particles are typically hydrophobic; however, they may undergo aging processes during their transport, which may change their surface properties and make them capable of acting as CCNs.

Table 2. Overview of the AERONET sites used for comparing the dust-related CCNC from POLIPHON and OMCAM. The total number of data points for each site is derived from the AERONET Level-1.5 aerosol inversion product.

305

310

	AERONET site name	City name	Location	$c_{100,d}$ (cm ⁻³ for α_d =1 Mm ⁻¹)	$\chi_{ m d}$	Dust-presence / total data point number
North America	La_Parguera	La Parguera, Puerto Rico	17.97°N, 67.05°W	1.68±1.02	0.81±0.01	2005/12068
	Fresno_2	Fresno, USA	36.79°N, 119.77°W	3.21±1.19	0.84±0.08	149/105535
South America	CEILAP-BA	Buenos Aires, Argentina	34.56°S, 58.51°W	3.25±1.18	0.93±0.07	123/11433
	Trelew	Trelew, Argentina	43.25°S, 65.31°W	1.41±1.22	0.81±0.07	133/9240
Africa	Cairo_EMA_2	Cairo, Egypt	30.08°N, 31.29°E	2.79±1.03	0.76±0.03	1959/11919
	IER_Cinzana	IER-Cinzana, Mali	13.28°N, 5.93°W	2.11±1.06	0.82±0.04	10633/14269
	Zinder_Airport	Zinder, Niger	13.77°N, 8.99°E	3.01±1.04	0.92±0.03	7063/9867
Middle East	KAUST_Campus	Thuwal, Saudi Arabia	22.30°N, 39.10°E	3.27±1.02	0.90±0.02	5294/17022
East Asia	Beijing	Beijing, China	39.98°N, 116.38°E	3.52±1.15	1.01±0.10	545/14409
Australia	Birdsville	Birdsville, Australia	25.90°S, 139.35°E	2.34±1.14	1.05±0.05	371/11569
Europe	Granada	Granada, Spain	37.16°N, 3.61°W	2.76±1.03	0.70±0.02	2670/20983
	Palma_de_Mallorca	Palma de Mallorca, Spain	39.55°N, 2.63°E	3.59±1.09	0.85±0.03	1207/11652

Figure 7 presents the average dust-related CCNC profiles at a supersaturation of 0.2% with respect to liquid water from the POLIPHON and OMCAM methods, respectively, at the 12 sites listed in Table 2. CCNC values from OMCAM are generally larger than those from POLIPHON with a difference of less than one order of magnitude. The overall uncertainty in OMCAM-derived CCNC is estimated to be 200%-300% (Choudhury and Tesche, 2023a), whereas the uncertainty in POLIPHON-derived CCNC ranges from 50% to 200% (Ansmann et al., 2019a). As a result, even differences as large as an order of magnitude can still be considered acceptable within the uncertainty bound, particularly for a parameter like CCNC, which can vary by more than five orders of magnitude at a given location (Choudhury and Tesche, 2022b).

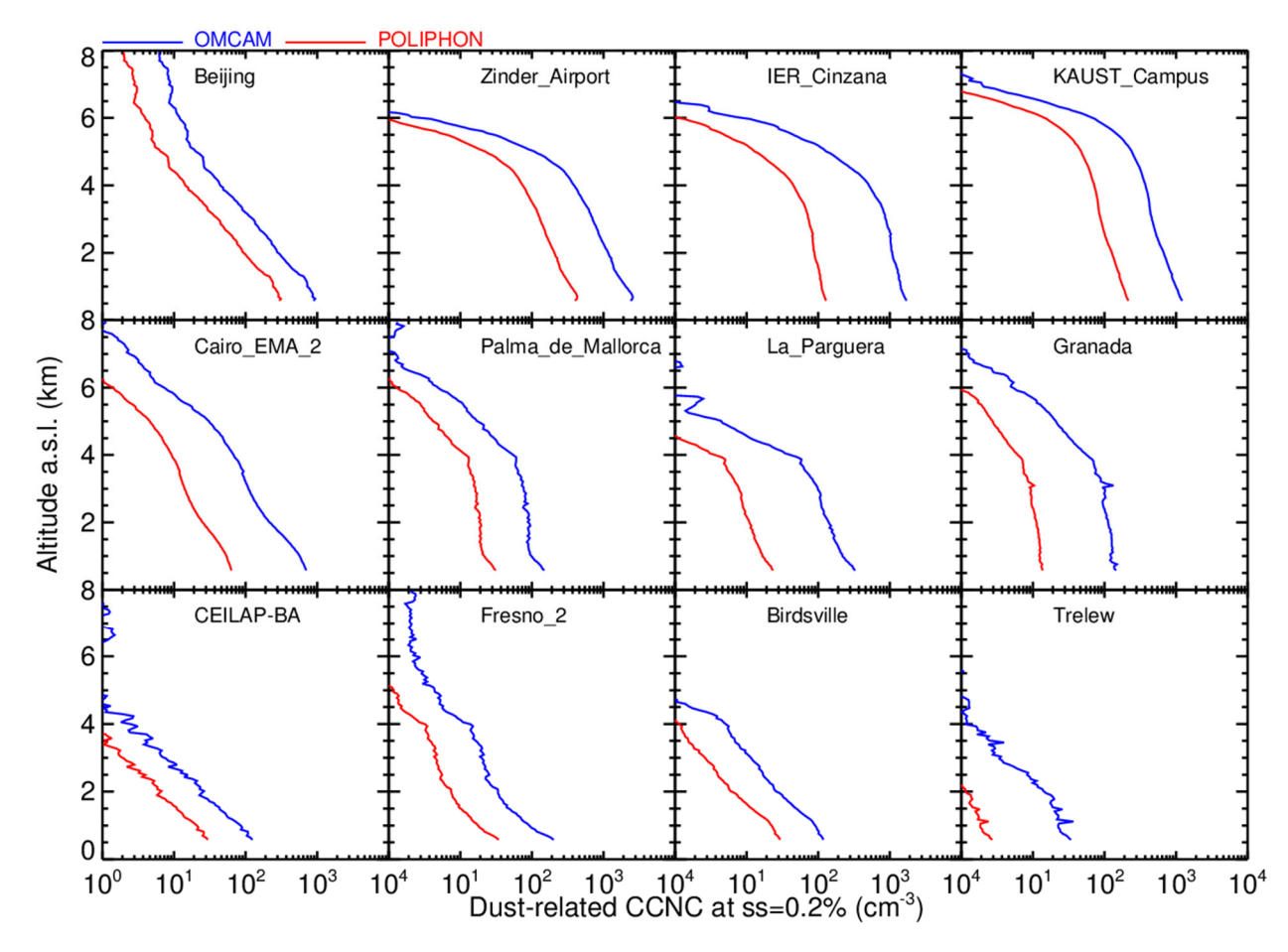


Figure 7. Dust-related CCNC (at a water supersaturation ss=0.2%) profiles derived using POLIPHON (red) and OMCAM (blue) at 12 selected AERONET sites. Profiles represent the average from June 2006 to December 2021 and are based on monthly means.

320

325

330

The comparison also suggests that the globally fixed dust PSD defined by the CALIPSO aerosol model may not accurately depict the dust microphysical properties at these locations. The site-average dust-related PSDs in Figure 8a highlight the dominance of coarse-mode particles at the selected sites though significant differences in maximum concentration are visible between sites. Figure 8b presents the normalized particle volume size distribution provided in the CALIPSO aerosol model, which is used in OMCAM retrieval, together with the twelve-site average particle volume size distributions for different dust identification schemes ($R_{d,1020nm} \ge 80\%$ and 89%). If the dust fraction in the atmospheric column increases, the number of coarse-mode dust particles rapidly increase. Differences between CCNC values from POLIPHON and OMCAM may arise from site-to-site variations of dust microphysical properties, such as particle size distribution, refractive index, and lidar ratio due to gravitational deposition along the dust transport pathway from dust sources (Ansmann et al., 2017; Ratcliffe et al., 2024). Compared with the average PSDs of identified dust data (see Figure 8b), the CALIPSO aerosol model dust PSD exhibits a similar mean radius for both the fine and coarse modes (μ_f and μ_c). However, significant differences are observed in the volume fraction of the coarse and fine mode (v_f and v_c) between the identified dust PSDs and the fixed normalized dust PSD from the CALIPSO aerosol model. It is evident that the coarse-to-fine mode particle ratios are much higher for the identified dust data in this study compared to those from the CALIPSO aerosol model applied in OMCAM. This implies that when using the fixed dust PSD in OMCAM to reproduce CALIOP-derived aerosol extinction, a larger number concentration of fine-mode dust particles is produced, leading to a higher $n_{100,d}$, and thus, a higher dust CCNC value. Moreover, the varying influence of local aerosols is also contributed since dust-dominant mixture data points from AERONET are applied in this study.

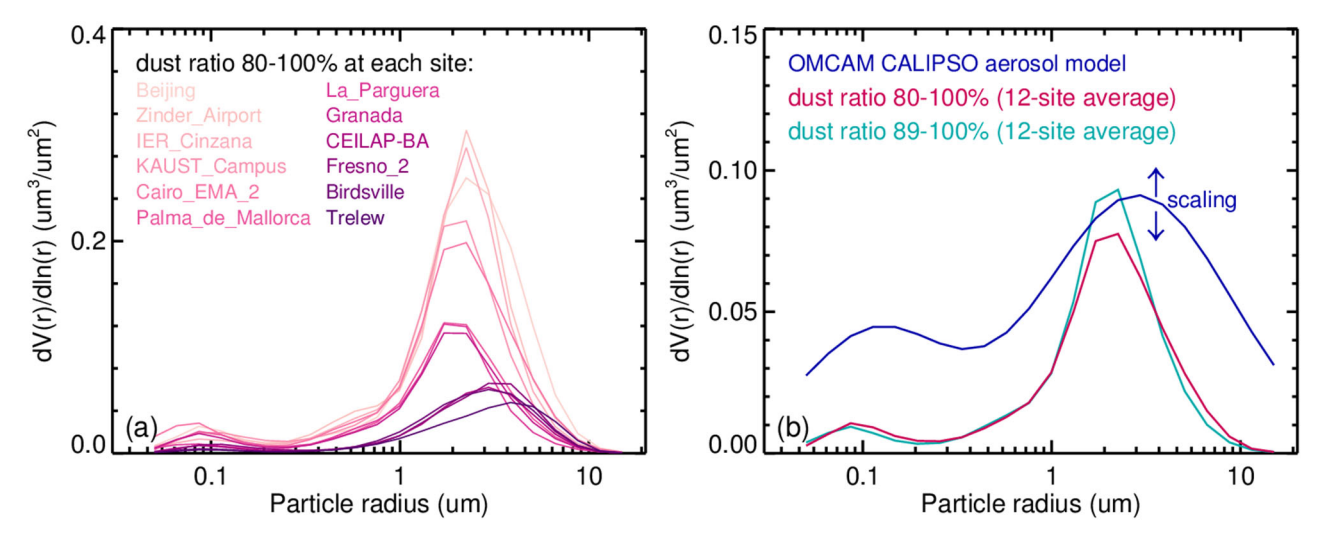


Figure 8. (a) Dust column-integrated particle volume size distributions at the selected AERONET sites from AERONET aerosol inversion data product identified using the columnar dust ratio $R_{\rm d,1020nm}$ threshold of \geq 80%. (b) Average column-integrated particle volume size distributions of the twelve selected sites with the columnar dust ratio $R_{\rm d,1020nm}$ thresholds of \geq 80% (in magenta) and \geq 89%. (in cyan, as used in He et al. (2023)), and the normalized particle volume size distribution for dust from the CALIPSO aerosol model (in blue), which is used to reproduce the CALIOP-derived dust extinctions by multiplying a scaling factor in OMCAM. The standard deviations ($\sigma_{\rm f}$ and $\sigma_{\rm c}$) are 1.4813 μ m and 1.9078 μ m for fine and coarse mode, respectively; the volume fractions ($\nu_{\rm f}$ and $\nu_{\rm c}$) are 0.223 and 0.777 for fine and coarse mode, respectively; the mean radii ($\mu_{\rm f}$ and $\mu_{\rm c}$) are 0.1165 μ m and 2.8329 μ m for fine and coarse mode, respectively (Choudhury and Tesche, 2023a).

The current Version 4 CALIOP retrievals rely on globally constant, aerosol-type-specific lidar ratios that are directly linked to fixed, associated normalized PSDs (Kim et al., 2018). Therefore, incorporating the aforementioned variations into a CCNC-retrieval algorithm for CALIOP is challenging, since these normalized PSDs can only be scaled, without modifying their shape or the coarse-to-fine particle number ratios. This emphasizes the need for in-situ and remote sensing campaigns measuring dust aerosols across different regions (Ansmann et al., 2009; Ryder et al., 2013, 2018; Weinzierl et al., 2009, 2017; Haarig et al., 2017). Recent measurements from the past 15 years have not been incorporated into the CALIPSO aerosol model (Omar et al., 2009), underscoring the regional complexity of dust aerosols and suggesting that coarse-mode dust particles may be underestimated in the current model (Ansmann et al., 2017; Kok et al., 2021; Adebiyi et al., 2023; Ratcliffe et al., 2024). This conclusion is consistent with the results shown in Figure 8, suggesting an underestimation of the coarse-to-fine dust particle number ratio. The upcoming Version 5 CALIOP data product is expected to include regionally varying lidar ratios in its aerosol-retrieval algorithm (Haarig et al., 2025), which will improve the accuracy of the Level-2 dust extinction coefficient, an essential input for dust CCNC retrieval. However, our results also highlight the importance of accounting for regional variations in the microphysical properties of dust (and other aerosol types) when updating OMCAM or developing other future algorithms that are used for global CCNC retrieval from spaceborne lidar measurements. Considering such regional variations in dust microphysics is crucial for the broader applications of spaceborne lidar-derived height-resolved CCNC datasets in ACI studies.

5. Summary and conclusions

335

340

345

350

355

360

Obtaining the global height-resolved distribution of CCNC and INPC from lidar observations marks a promising pathway for ACI studies. However, the POLIPHON method requires aerosol-type-specific and regional varying conversion factors for transforming optical parameters from lidar measurements into cloud-relevant aerosol concentrations.

Here, we extend our earlier work to obtain an extended dataset of 532-nm dust-related conversion factors at 198 AERONET sites. This includes mass- and INP-relevant conversion factors at 137 sites and CCN-relevant conversion factors at 123 sites.

The geographical distribution of these sites ensures that major deserts and routes of dust transport are now represented by corresponding conversion factors. We find regional variations in dust-related conversion factors that suggest changes in dust microphysical properties along the transport pathways of dust plumes. For instance, differences in the gravitational settling of fine and coarse dust modulate the shape of the PSD during the transport. Moreover, the varying levels of mixing with other aerosols might contribute to regional variations of the conversion factors since our relaxed criterion for identifying dust presence may lead to the inclusion of non-dust particles. In general, $c_{\rm v,d}$ tends to decrease with greater distance from dust sources. In contrast, $c_{250,\rm d}$, $c_{\rm s,d}$, and $c_{\rm s,100,\rm d}$ are found to be larger downstream of desert regions. The CCN-relevant conversion factors $c_{100,\rm d}$ and $\chi_{\rm d}$ show site-to-site variations without a clear regional pattern, because they are more sensitive to the contribution of local fine-mode particles. Overall, our findings highlight the importance of considering geographic variations in dust-related conversion factors for inferring dust-related particle concentrations from lidar observations.

365

370

375

380

385

390

395

400

405

Note that compiling a gridded dust conversion factor dataset is challenging, although such a data set would be highly useful for future studies of global ACI. This arises from the limited number of available sites relative to global coverage, as well as their inhomogeneous geographical distribution. We recommend using values from the nearest available site when applying the current conversion factor dataset.

To test the performance of the derived conversion factors, we conduct a comparison of CALIOP-based dust-related CCNC profiles by applying the POLIPHON and OMCAM methods to data collected at 12 AERONET sites. We generally find agreement within an order of magnitude, which is acceptable given the respective retrieval uncertainties (Choudhury and Tesche, 2023a; Ansmann et al., 2019a). It is most likely that site-to-site variations in dust microphysical properties contribute to these differences. OMCAM employs a single fixed dust PSD from the CALIPSO aerosol model, while POLIPHON uses climatology-based conversion factors that account for regional variations in dust PSD. The most notable difference is that the PSDs of the identified dust data in this study show much higher coarse-to-fine dust particle number ratios compared to the fixed dust PSD used by CALIPSO. This difference contributes to a much higher number concentration of fine particles for OMCAM to reconstruct a similar particle extinction coefficient, and finally leads to higher dust CCNC values compared with POLIPHON. As a consequence, discrepancies in CCNC profiles between the two methods partly reflect the inadequate representativeness of the CALIPSO-model-defined dust PSD at different locations. It is a trade-off for the current version of OMCAM to use the globally fixed, aerosol-type-specific PSDs to retrieve a reasonably accurate CCNC dataset, given the limitations of the current Version 4 CALIOP retrievals. Nevertheless, additional in situ measurements will be essential in the future to validate the capability of both POLIPHON and OMCAM in retrieving global dust CCNC climatology. Therefore, further efforts are needed in incorporating regional-dependent microphysics of dust (and other aerosol types) to improve the OMCAM algorithm, for its broader applicability to ACI studies on a global scale.

We have tested the conversion factors by comparing the derived CCNC profiles with CCNC profiles generated by OMCAM retrievals. In the future, it is also necessary to validate the conversion factor dataset by comparing the retrieved CCNC and INPC (or INP-relevant parameters such as $n_{250,d}$ and s_d) profiles with other independent, co-located, and simultaneous data, from either model outputs (Chatziparaschos et al., 2024; Herbert et al., 2025), in situ measurements (Haarig et al., 2019; Marinou et al., 2019; Kezoudi et al., 2021; Lenhardt et al., 2023), or airborne lidar measurements (Müller et al., 2014). Furthermore, the newly launched EarthCARE ATLID (Atmospheric LIDar) spaceborne lidar also requires conversion factors at 355 nm (Wehr et al., 2023), which can also be calculated with our method. Given the increasing use of ceilometers, extending the conversion factor dataset to a wavelength of 910 nm is also of interest. In addition to dust, conversion factors for other aerosol types (e.g., smoke, volcanic aerosol, sea spray aerosol, anthropogenic aerosol, and so on), as well as their regional-variation features should also be estimated to further extend the applicability of the POLIPHON method in estimating height-resolved CCNC, which is a key parameter to improve our understanding of ACI (Tan et al., 2014; Ansmann et al., 2021; Córdoba et al., 2021).

Data availability

410

415

420

425

435

AERONET data used in this work can be accessed at https://aeronet.gsfc.nasa.gov/ (AERONET, 2023a, 2023b); CALIPSO aerosol profile product can be downloaded at https://subset.larc.nasa.gov/ (CALIPSO, 2025); OMCAM CCNC dataset can be accessed via the link: https://doi.org/10.1594/PANGAEA.956215 (Choudhury and Tesche, 2023b).

Author contributions

Yun He conceived the research, analyzed the data, acquired the research funding, and wrote the manuscript. Goutam Choudhury analyzed the data, participated in scientific discussions, and proofread the manuscript. Matthias Tesche, Albert Ansmann, and Detlef Müller reviewed the manuscript and participated in scientific discussions. Fan Yi acquired the research funding and led the study. Zhenping Yin participated in scientific discussions and data analysis.

Competing interests

The authors declare that they have no conflict of interest.

Financial support

This work was supported in part by the National Key Research and Development Program of China under Grant 2023YFC3007802. This research has also been supported by the National Natural Science Foundation of China (grant nos. 42005101, 41927804, and 42205130), the Natural Science Foundation of Hubei Province (grant no. 2023AFB617), the Chinese Scholarship Council (CSC) (grant no. 202206275006), and the Meridian Space Weather Monitoring Project (China). Goutam Choudhury was supported by the German Research Foundation (Deutsche Forschungsgemeinschaft, DFG; grant no. 524386224). Matthias Tesche has been supported by the Federal State of Saxony and the European Social Fund (ESF, grant no. 100649813).

Acknowledgements

The authors thank all PIs of the AERONET sites used in this study for maintaining their instruments and providing their data to the community, and the Atmospheric Science Data Central at the NASA (National Aeronautics and Space Administration) Langley Research Center for providing the CALIPSO data.

430 References

- Adebiyi, A. A., Kok, J. F., Wang, Y., Ito, A., Ridley, D. A., Nabat, P., and Zhao, C.: Dust Constraints from joint Observational-Modelling-experiMental analysis (DustCOMM): comparison with measurements and model simulations, Atmos. Chem. Phys., 20, 829–863, https://doi.org/10.5194/acp-20-829-2020, 2020.
- Adebiyi, A., Kok, J. F., Murray, B. J., Ryder, C. L., Stuut, J.-B. W., Kahn, R. A., Knippertz, P., Formenti, P., Mahowald, N. M., Pérez García-Pando, C., Klose, M., Ansmann, A., Samset, B. H., Ito, A., Balkanski, Y., Di Biagio, C., Romanias, M. N., Huang, Y., and Meng, J.: A review of coarse mineral dust in the Earth system, Aeolian Res., 60, 100849, https://doi.org/10.1016/j.aeolia.2022.100849, 2023.
 - AERONET: AERONET Aerosol Optical Depth (V3) Solar data base, Aerosol Robotic Network [data set], https://aeronet.gsfc.nasa.gov/new_web/download_all_v3_aod.html, last access: 12 April 2023a.

- 440 AERONET: AERONET Aerosol Inversion (V3) data base, Aerosol Robotic Network [data set], https://aeronet.gsfc.nasa.gov/new_web/download_all_v3_inversions.html, last access: 12 April 2023b.
 - Alexandri, F., Müller, F., Choudhury, G., Achtert, P., Seelig, T., and Tesche, M.: A cloud-by-cloud approach for studying aerosol-cloud interaction in satellite observations, Atmos. Meas. Tech., 17, 1739–1757, https://doi.org/10.5194/amt-17-1739-2024, 2024.
- Ansmann, A., Tesche, M., Knippertz, P., Bierwirth, E., Althausen, D., Müller, D., Schulz, O.: Vertical profiling of convective dust plumes in southern Morocco during SAMUM, Tellus B: Chem. Phys. Meteorol., 61, 340–353, https://doi.org/10.1111/j.1600-0889.2008.00384.x, 2009.
 - Ansmann, A., Rittmeister, F., Engelmann, R., Basart, S., Jorba, O., Spyrou, C., Remy, S., Skupin, A., Baars, H., Seifert, P., Senf, F., and Kanitz, T.: Profiling of Saharan dust from the Caribbean to western Africa Part 2: Shipborne lidar measurements versus forecasts, Atmos. Chem. Phys., 17, 14987–15006, https://doi.org/10.5194/acp-17-14987-2017, 2017.

- Ansmann, A., Mamouri, R.-E., Hofer, J., Baars, H., Althausen, D., and Abdullaev, S. F.: Dust mass, cloud condensation nuclei, and ice-nucleating particle profiling with polarization lidar: updated POLIPHON conversion factors from global AERONET analysis, Atmos. Meas. Tech., 12, 4849–4865, https://doi.org/10.5194/amt-12-4849-2019, 2019a.
- Ansmann, A., Mamouri, R.-E., Bühl, J., Seifert, P., Engelmann, R., Hofer, J., Nisantzi, A., Atkinson, J. D., Kanji, Z. A., Sierau, B., Vrekoussis, M., and Sciare, J.: Ice-nucleating particle versus ice crystal number concentration in altocumulus and cirrus layers embedded in Saharan dust: a closure study, Atmos. Chem. Phys., 19, 15087–15115, https://doi.org/10.5194/acp-19-15087-2019, 2019b.
- Ansmann, A., Ohneiser, K., Mamouri, R.-E., Knopf, D. A., Veselovskii, I., Baars, H., Engelmann, R., Foth, A., Jimenez, C.,

 Seifert, P., and Barja, B.: Tropospheric and stratospheric wildfire smoke profiling with lidar: mass, surface area, CCN, and INP retrieval, Atmos. Chem. Phys., 21, 9779–9807, https://doi.org/10.5194/acp-21-9779-2021, 2021.
 - Aravindhavel, A., Choudhury, G., Prabhakaran, T., Murugavel, P., and Tesche, M.: Retrieval and validation of cloud condensation nuclei from satellite and airborne measurements over the Indian Monsoon region, Atmos. Res., 290, 106 802, https://doi.org/10.1016/j.atmosres.2023.106802, 2023.
- Baars, H., Kanitz, T., Engelmann, R., Althausen, D., Heese, B., Komppula, M., Preißler, J., Tesche, M., Ansmann, A., Wandinger, U., Lim, J.-H., Ahn, J. Y., Stachlewska, I. S., Amiridis, V., Marinou, E., Seifert, P., Hofer, J., Skupin, A., Schneider, F., Bohlmann, S., Foth, A., Bley, S., Pfüller, A., Giannakaki, E., Lihavainen, H., Viisanen, Y., Hooda, R. K., Pereira, S. N., Bortoli, D., Wagner, F., Mattis, I., Janicka, L., Markowicz, K. M., Achtert, P., Artaxo, P., Pauliquevis, T., Souza, R. A. F., Sharma, V. P., van Zyl, P. G., Beukes, J. P., Sun, J., Rohwer, E. G., Deng, R., Mamouri, R.-E., and Zamorano, F.: An overview of the first decade of Polly^{NET}: an emerging network of automated Raman-polarization lidars for continuous aerosol profiling, Atmos. Chem. Phys., 16, 5111–5137, https://doi.org/10.5194/acp-16-5111-2016, 2016.
 - Bullard, J. E., Baddock, M., Bradwell, T., Crusius, J., Darlington, E., Gaiero, D., Gassó, S., Gisladottir, G., Hodgkins, R., McCulloch, R., McKenna-Neuman, C., Mockford, T., Stewart, H., and Thorsteinsson, T.: High-latitude dust in the Earth system, Rev. Geophys., 54, 447–485, https://doi.org/10.1002/2016RG000518, 2016.
- 475 CALIPSO: Cloud–Aerosol lidar and infrared pathfinder satellite observation data base [data set]. https://subset.larc.nasa.gov/, last access: 28 January 2025.
 - Casquero-Vera, J. A., Pérez-Ramírez, D., Lyamani, H., Rejano, F., Casans, A., Titos, G., Olmo, F. J., Dada, L., Hakala, S., Hussein, T., Lehtipalo, K., Paasonen, P., Hyvärinen, A., Pérez, N., Querol, X., Rodríguez, S., Kalivitis, N., González, Y., Alghamdi, M. A., Kerminen, V.-M., Alastuey, A., Petäjä, T., and Alados-Arboledas, L.: Impact of desert dust on new particle formation events and the cloud condensation nuclei budget in dust-influenced areas, Atmos. Chem. Phys., 23, 15795–15814, https://doi.org/10.5194/acp-23-15795-2023, 2023.

- Chatziparaschos, M., Myriokefalitakis, S., Kalivitis, N., Daskalakis, N., Nenes, A., Gonçalves Ageitos, M., Costa-Surós, M., Pérez García-Pando, C., Vrekoussis, M., and Kanakidou, M.: Assessing the global contribution of marine, terrestrial bioaerosols, and desert dust to ice-nucleating particle concentrations, EGUsphere [preprint], https://doi.org/10.5194/egusphere-2024-952, 2024.
 - Chen, S., Chen, J., Zhang, Y., Lin, J., Bi, H., Song, H., Chen, Y., Lian, L., Liu, C., and Zhang, R.: Anthropogenic dust: Sources, characteristics and emissions, Environ. Res. Lett., 18, 103002. https://doi.org/10.1088/1748-9326/acf479, 2023.
 - Choudhury, G. and Tesche, M.: Estimating cloud condensation nuclei concentrations from CALIPSO lidar measurements, Atmos. Meas. Tech., 15, 639–654, https://doi.org/10.5194/amt-15-639-2022, 2022a.
- Choudhury, G. and Tesche, M.: Assessment of CALIOP-derived CCN concentrations by in situ surface measurements, Remote Sens., 14, 3342, https://doi.org/10.3390/rs14143342, 2022b.
 - Choudhury, G., Ansmann, A., and Tesche, M.: Evaluation of aerosol number concentrations from CALIPSO with ATom airborne in situ measurements, Atmos. Chem. Phys., 22, 7143–7161, https://doi.org/10.5194/acp-22-7143-2022, 2022.
 - Choudhury, G. and Tesche, M.: A first global height-resolved cloud condensation nuclei data set derived from spaceborne lidar measurements, Earth Syst. Sci. Data, 15, 3747–3760, https://doi.org/10.5194/essd-15-3747-2023, 2023a.

500

510

515

- Choudhury, G. and Tesche, M.: Global multiyear 3D dataset of cloud condensation nuclei derived from spaceborne lidar measurements, PANGAEA [data set], https://doi.org/10.1594/PANGAEA.956215, 2023b.
- Choudhury, G., Block, K., Haghighatnasab, M., Quaas, J., Goren, T., and Tesche, M.: Pristine oceans are a significant source of uncertainty in quantifying global cloud condensation nuclei, Atmos. Chem. Phys., 25, 3841–3856, https://doi.org/10.5194/acp-25-3841-2025, 2025.
- Córdoba, F., Ramírez-Romero, C., Cabrera, D., Raga, G. B., Miranda, J., Alvarez-Ospina, H., Rosas, D., Figueroa, B., Kim, J. S., Yakobi-Hancock, J., Amador, T., Gutierrez, W., García, M., Bertram, A. K., Baumgardner, D., and Ladino, L. A.: Measurement report: Ice nucleating abilities of biomass burning, African dust, and sea spray aerosol particles over the Yucatán Peninsula, Atmos. Chem. Phys., 21, 4453–4470, https://doi.org/10.5194/acp-21-4453-2021, 2021.
- DeMott, P. J., Prenni, A. J., McMeeking, G. R., Sullivan, R. C., Petters, M. D., Tobo, Y., Niemand, M., Möhler, O., Snider, J. R., Wang, Z., and Kreidenweis, S. M.: Integrating laboratory and field data to quantify the immersion freezing ice nucleation activity of mineral dust particles, Atmos. Chem. Phys., 15, 393–409, https://doi.org/10.5194/acp-15-393-2015, 2015.
 - Fernald, F. G.: Analysis of atmospheric lidar observations: some comments, Appl. Optics, 23, 652–653, https://doi.org/10.1364/AO.23.000652, 1984.
 - Floutsi, A. A., Baars, H., Engelmann, R., Althausen, D., Ansmann, A., Bohlmann, S., Heese, B., Hofer, J., Kanitz, T., Haarig, M., Ohneiser, K., Radenz, M., Seifert, P., Skupin, A., Yin, Z., Abdullaev, S. F., Komppula, M., Filioglou, M., Giannakaki, E., Stachlewska, I. S., Janicka, L., Bortoli, D., Marinou, E., Amiridis, V., Gialitaki, A., Mamouri, R.-E., Barja, B., and Wandinger, U.: DeLiAn a growing collection of depolarization ratio, lidar ratio and Ångström exponent for different aerosol types and mixtures from ground-based lidar observations, Atmos. Meas. Tech., 16, 2353–2379, https://doi.org/10.5194/amt-16-2353-2023, 2023.
 - Freudenthaler, V., Esselborn, M., Wiegner, M., Heese, B., Tesche, M., Ansmann, A., Müller, D., Althausen, D., Wirth, M., Fix, A., Ehret, G., Knippertz, P., Toledano, C., Gasteiger, J., Garhammer, M., and Seefeldner, M.: Depolarization ratio profil-ing at several wavelengths in pure Saharan dust during SAMUM2006, Tellus B, 61(1), 165-179. https://doi.org/10.1111/j.1600-0889.2008.00396.x, 2009.
 - Gasteiger, J. and Wiegner, M.: MOPSMAP v1.0: a versatile tool for the modeling of aerosol optical properties, Geosci. Model Dev., 11, 2739–2762, https://doi.org/10.5194/gmd-11-2739-2018, 2018.
 - Georgoulias, A. K., Marinou, E., Tsekeri, A., Proestakis, E., Akritidis, D., Alexandri, G., Zanis, P., Balis, D., Marenco, F.,

Tesche, M., and Amiridis, V.: A first case study of CCN concentrations from spaceborne lidar observations, Remote Sens., 12, 1557, https://doi.org/10.3390/rs12101557, 2020.

530

- Giles, D. M., Sinyuk, A., Sorokin, M. G., Schafer, J. S., Smirnov, A., Slutsker, I., Eck, T. F., Holben, B. N., Lewis, J. R., Campbell, J. R., Welton, E. J., Korkin, S. V., and Lyapustin, A. I.: Advancements in the Aerosol Robotic Network (AERONET) Version 3 database automated near-real-time quality control algorithm with improved cloud screening for Sun photometer aerosol optical depth (AOD) measurements, Atmos. Meas. Tech., 12, 169–209, https://doi.org/10.5194/amt-12-169-2019, 2019.
- Haarig, M., Ansmann, A., Althausen, D., Klepel, A., Groß, S., Freudenthaler, V., Toledano, C., Mamouri, R.-E., Farrell, D. A., Prescod, D. A., Marinou, E., Burton, S. P., Gasteiger, J., Engelmann, R., and Baars, H.: Triple-wavelength depolarization-ratio profiling of Saharan dust over Barbados during SALTRACE in 2013 and 2014, Atmos. Chem. Phys., 17, 10767–10794, https://doi.org/10.5194/acp-17-10767-2017, 2017.
- Haarig, M., Walser, A., Ansmann, A., Dollner, M., Althausen, D., Sauer, D., Farrell, D., and Weinzierl, B.: Profiles of cloud condensation nuclei, dust mass concentration, and ice-nucleating-particle-relevant aerosol properties in the Saharan Air Layer over Barbados from polarization lidar and airborne in situ measurements, Atmos. Chem. Phys., 19, 13773–13788, https://doi.org/10.5194/acp-19-13773-2019, 2019.
- Haarig, M., Ansmann, A., Engelmann, R., Baars, H., Toledano, C., Torres, B., Althausen, D., Radenz, M., and Wandinger, U.:
 First triple-wavelength lidar observations of depolarization and extinction-to-backscatter ratios of Saharan dust, Atmos.
 Chem. Phys., 22, 355–369, https://doi.org/10.5194/acp-22-355-2022, 2022.
 - Haarig, M., Engelmann, R., Baars, H., Gast, B., Althausen, D., and Ansmann, A.: Discussion of the spectral slope of the lidar ratio between 355 and 1064 nm from multiwavelength Raman lidar observations, Atmos. Chem. Phys., 25, 7741–7763, https://doi.org/10.5194/acp-25-7741-2025, 2025.
- Han, Y., Wang, T., Tang, J., Wang, C., Jian, B., Huang, Z., and Huang, J.: New insights into the Asian dust cycle derived from CALIPSO lidar measurements, Remote Sens. Environ., 272, 112906, https://doi.org/10.1016/j.rse.2022.112906, 2022.
 - Herbert, R. J., Sanchez-Marroquin, A., Grosvenor, D. P., Pringle, K. J., Arnold, S. R., Murray, B. J., and Carslaw, K. S.: Gaps in our understanding of ice-nucleating particle sources exposed by global simulation of the UK Earth System Model, Atmos. Chem. Phys., 25, 291–325, https://doi.org/10.5194/acp-25-291-2025, 2025.
- He, Y., Yi, F., Yi, Y., Liu, F., and Zhang, Y.: Heterogeneous nucleation of midlevel cloud layer influenced by transported Asian dust over Wuhan (30.5°N, 114.4°E), China, J. Geophys. Res.-Atmos., 126, e2020JD033394, https://doi.org/10.1029/2020JD033394, 2021a.
 - He, Y., Zhang, Y., Liu, F., Yin, Z., Yi, Y., Zhan, Y., and Yi, F.: Retrievals of dust-related particle mass and ice-nucleating particle concentration profiles with ground-based polarization lidar and sun photometer over a megacity in central China, Atmos. Meas. Tech., 14, 5939–5954, https://doi.org/10.5194/amt-14-5939-2021, 2021b.
 - He, Y., Yin, Z., Liu, F., and Yi, F.: Technical note: Identification of two ice-nucleating regimes for dust-related cirrus clouds based on the relationship between number concentrations of ice-nucleating particles and ice crystals, Atmos. Chem. Phys., 22, 13067–13085, https://doi.org/10.5194/acp-22-13067-2022, 2022.
- He, Y., Yin, Z., Ansmann, A., Liu, F., Wang, L., Jing, D., and Shen, H.: POLIPHON conversion factors for retrieving dust-related cloud condensation nuclei and ice-nucleating particle concentration profiles at oceanic sites, Atmos. Meas. Tech., 16, 1951–1970, https://doi.org/10.5194/amt-16-1951-2023, 2023.
 - He, Y.: An extended POLIPHON conversion factor dataset for dust [data set]. Zenodo. https://doi.org/10.5281/zenodo.16781089, 2025. (last access: 8 August 2025)
- Hofer, J., Althausen, D., Abdullaev, S. F., Makhmudov, A. N., Nazarov, B. I., Schettler, G., Engelmann, R., Baars, H., Fomba, K. W., Müller, K., Heinold, B., Kandler, K., and Ansmann, A.: Long-term profiling of mineral dust and pollution aerosol

- with multiwavelength polarization Raman lidar at the Central Asian site of Dushanbe, Tajikistan: case studies, Atmos. Chem. Phys., 17, 14559–14577, https://doi.org/10.5194/acp-17-14559-2017, 2017.
- Hofer, J., Ansmann, A., Althausen, D., Engelmann, R., Baars, H., Abdullaev, S. F., and Makhmudov, A. N.: Long-term profiling of aerosol light extinction, particle mass, cloud condensation nuclei, and ice-nucleating particle concentration over Dushanbe, Tajikistan, in Central Asia, Atmos. Chem. Phys., 20, 4695–4711, https://doi.org/10.5194/acp-20-4695-2020, 2020.
 - Holben, B., Eck, T., Slutsker, I., Tanré, D., Buis, J., Setzer, A., Vermote, E., Reagan, J., Kaufman, Y., Nakajima, T., Lavenu, F., Jankowiak, I., and Smirnov, A.: AERONET A federated instrument network and data archive for aerosol characterization, Remote Sens. Environ., 66, 1–16, https://doi.org/10.1016/s0034-4257(98)00031-5, 1998.
- Hu, Q., Wang, H., Goloub, P., Li, Z., Veselovskii, I., Podvin, T., Li, K., and Korenskiy, M.: The characterization of Taklamakan dust properties using a multiwavelength Raman polarization lidar in Kashi, China, Atmos. Chem. Phys., 20, 13817–13834, https://doi.org/10.5194/acp-20-13817-2020, 2020.

595

- Hu, Z., Huang, J., Zhao, C., Ma, Y., Jin, Q., Qian, Y., Leung, L. R., Bi, J., and Ma, J.: Trans-Pacific transport and evolution of aerosols: spatiotemporal characteristics and source contributions, Atmos. Chem. Phys., 19, 12709–12730, https://doi.org/10.5194/acp-19-12709-2019, 2019.
- Huang, J., Minnis, P., Lin, B., Wang, T., Yi, Y., Hu, Y., Sun-Mack, S., and Ayers, K.: Possible influences of Asian dust aerosols on cloud properties and radiative forcing observed from MODIS and CERES, Geophys. Res. Lett., 33, L06824, https://doi.org/10.1029/2005GL024724, 2006.
- IPCC, 2021: Climate Change 2021: The Physical Science Basis. Contribution of Working Group I to the Sixth Assessment
 Report of the Intergovernmental Panel on Climate Change [Masson-Delmotte, V., P. Zhai, A. Pirani, S.L. Connors, C.
 Péan, S. Berger, N. Caud, Y. Chen, L. Goldfarb, M.I. Gomis, M. Huang, K. Leitzell, E. Lonnoy, J.B.R. Matthews, T.K.
 Maycock, T. Waterfield, O. Yelekçi, R. Yu, and B. Zhou (eds.)]. Cambridge University Press, Cambridge, United
 Kingdom and New York, NY, USA, In press, doi:10.1017/9781009157896, 2021.
- Jing, D., He, Y., Yin, Z., Liu, F., and Yi, F.: Long-term characteristics of dust aerosols over central China from 2010 to 2020 observed with polarization lidar, Atmos. Res., 297, 107129, https://doi.org/10.1016/j.atmosres.2023.107129, 2024.
 - Kai, K., Kawai, K., Ohara, K., Minamoto, Y., Jin, Y., Maki, T., Noda, J., Shiina, T., and Davaanyam, E.: Mass-Extinction Conversion Factor (MECF) over the Gobi Desert by a Tethered-balloon-based OPC and a Ceilometer, SOLA, 19, 269-273, https://doi.org/10.2151/sola.2023-035, 2023.
 - Kanji, Z. A., Ladino, L. A., Wex, H., Boose, Y., Burkert-Kohn, M., Cziczo, D. J., and Krämer, M.: Overview of ice nucleating particles, Meteor. Mon., 58, 1.1–1.33, https://doi.org/10.1175/AMSMONOGRAPHS-D-16-0006.1, 2017.
 - Kezoudi, M., Tesche, M., Smith, H., Tsekeri, A., Baars, H., Dollner, M., Estellés, V., Bühl, J., Weinzierl, B., Ulanowski, Z., Müller, D., and Amiridis, V.: Measurement report: Balloon-borne in situ profiling of Saharan dust over Cyprus with the UCASS optical particle counter, Atmos. Chem. Phys., 21, 6781–6797, https://doi.org/10.5194/acp-21-6781-2021, 2021.
- Kim, M.-H., Omar, A. H., Tackett, J. L., Vaughan, M. A., Winker, D. M., Trepte, C. R., Hu, Y., Liu, Z., Poole, L. R., Pitts, M.
 C., Kar, J., and Magill, B. E.: The CALIPSO version 4 automated aerosol classification and lidar ratio selection algorithm,
 Atmos. Meas. Tech., 11, 6107–6135, https://doi.org/10.5194/amt-11-6107-2018, 2018.
 - Kok, J. F., Adebiyi, A. A., Albani, S., Balkanski, Y., Checa-Garcia, R., Chin, M., Colarco, P. R., Hamilton, D. S., Huang, Y., Ito, A., Klose, M., Leung, D. M., Li, L., Mahowald, N. M., Miller, R. L., Obiso, V., Pérez García-Pando, C., Rocha-Lima, A., Wan, J. S., and Whicker, C. A.: Improved representation of the global dust cycle using observational constraints on dust properties and abundance, Atmos. Chem. Phys., 21, 8127–8167, https://doi.org/10.5194/acp-21-8127-2021, 2021.
 - Korolev, A., McFarquhar, G., Field, P. R., Franklin, C., Lawson, P., Wang, Z., Williams, E., Abel, S. J., Axisa, D., Borrmann, S., Crosier, J., Fugal, J., Krämer, M., Lohmann, U., Schlenczek, O., Schnaiter, M., and Wendisch, M.: Mixed-Phase

- Clouds: Progress and Challenges, Meteor. Mon., 58, 5.1–5.50, https://doi.org/10.1175/AMSMONOGRAPHS-D-17-0001.1, 2017.
- 610 Lenhardt, E. D., Gao, L., Redemann, J., Xu, F., Burton, S. P., Cairns, B., Chang, I., Ferrare, R. A., Hostetler, C. A., Saide, P. E., Howes, C., Shinozuka, Y., Stamnes, S., Kacarab, M., Dobracki, A., Wong, J., Freitag, S., and Nenes, A.: Use of lidar aerosol extinction and backscatter coefficients to estimate cloud condensation nuclei (CCN) concentrations in the southeast Atlantic, Atmos. Meas. Tech., 16, 2037–2054, https://doi.org/10.5194/amt-16-2037-2023, 2023.
- Lv, M., Wang, Z., Li, Z., Luo, T., Ferrare, R., Liu, D., Wu, D., Mao, J., Wan, B., Zhang, F., and Wang, Y.: Retrieval of cloud condensation nuclei number concentration profiles from lidar extinction and backscatter data, J. Geophys. Res. Atmos., 123, 6082–6098, https://doi.org/10.1029/2017JD028102, 2018.
 - Mamouri, R. E. and Ansmann, A.: Fine and coarse dust separation with polarization lidar, Atmos. Meas. Tech., 7, 3717–3735, https://doi.org/10.5194/amt-7-3717-2014, 2014.
 - Mamouri, R. E. and Ansmann, A.: Estimated desert-dust ice nuclei profiles from polarization lidar: methodology and case studies, Atmos. Chem. Phys., 15, 3463–3477, https://doi.org/10.5194/acp-15-3463-2015, 2015.

625

- Mamouri, R.-E. and Ansmann, A.: Potential of polarization lidar to provide profiles of CCN- and INP-relevant aerosol parameters, Atmos. Chem. Phys., 16, 5905–5931, https://doi.org/10.5194/acp-16-5905-2016, 2016.
- Mamouri, R.-E., Ansmann, A., Ohneiser, K., Knopf, D. A., Nisantzi, A., Bühl, J., Engelmann, R., Skupin, A., Seifert, P., Baars, H., Ene, D., Wandinger, U., and Hadjimitsis, D.: Wildfire smoke triggers cirrus formation: lidar observations over the eastern Mediterranean, Atmos. Chem. Phys., 23, 14097–14114, https://doi.org/10.5194/acp-23-14097-2023, 2023.
- Marinou, E., Tesche, M., Nenes, A., Ansmann, A., Schrod, J., Mamali, D., Tsekeri, A., Pikridas, M., Baars, H., Engelmann, R., Voudouri, K.-A., Solomos, S., Sciare, J., Groß, S., Ewald, F., and Amiridis, V.: Retrieval of ice-nucleating particle concentrations from lidar observations and comparison with UAV in situ measurements, Atmos. Chem. Phys., 19, 11315–11342, https://doi.org/10.5194/acp-19-11315-2019, 2019.
- Mona, L., Amiridis, V., Cuevas, E., Gkikas, A., Trippetta, S., Vandenbussche, S., Benedetti, A., Dagsson-Waldhauserova, P., Formenti, P., Haefele, A., Kazadzis, S., Knippertz, P., Laurent, B., Madonna, F., Nickovic, S., Papagiannopoulos, N., Pappalardo, G., García-Pando, C. P., Popp, T., Rodríguez, S., Sealy, A., Sugimoto, N., Terradellas, E., Vimic, A. V., Weinzierl, B., and Basart, S.: Observing Mineral Dust in Northern Africa, the Middle East and Europe: Current Capabilities and Challenges Ahead for the Development of Dust Services, B. Am. Meteorol. Soc., 104, E2223–E2264, https://doi.org/10.1175/BAMS-D-23-0005.1, 2023.
 - Müller, D., Ansmann, A., Mattis, I., Tesche, M., Wandinger, U., Althausen, D., and Pisani, G.: Aerosol-type-dependent lidar ratios observed with Raman lidar, J. Geophys. Res., 112, D16202, https://doi.org/10.1029/2006JD008292, 2007.
 - Müller, D., Hostetler, C. A., Ferrare, R. A., Burton, S. P., Chemyakin, E., Kolgotin, A., Hair, J. W., Cook, A. L., Harper, D. B., Rogers, R. R., Hare, R. W., Cleckner, C. S., Obland, M. D., Tomlinson, J., Berg, L. K., and Schmid, B.: Airborne multiwavelength High Spectral Resolution Lidar (HSRL-2) observations during TCAP 2012: vertical profiles of optical and microphysical properties of a smoke/urban haze plume over the northeastern coast of the US, Atmos. Meas. Tech., 7, 3487–3496, https://doi.org/10.5194/amt-7-3487-2014, 2014.
 - Nakajima, T., Higurashi, A., Kawamoto, K., and Penner, J. E.: A possible correlation between satellite-derived cloud and aerosol microphysical parameters, Geophys. Res. Lett., 28(7), 1171–1174, https://doi.org/10.1029/2000GL012186, 2001.
- Noh, Y., Müller, D., Lee, K., Kim, K., Lee, K., Shimizu, A., Sano, I., and Park, C. B.: Depolarization ratios retrieved by AERONET sun–sky radiometer data and comparison to depolarization ratios measured with lidar, Atmos. Chem. Phys., 17, 6271–6290, https://doi.org/10.5194/acp-17-6271-2017, 2017.
 - Omar, A. H., Winker, D. M., Vaughan, M. A., Hu, Y., Trepte, C. R., Ferrare, R. A., Lee, K.-P., Hostetler, C. A., Kittaka, C., Rogers, R. R., Kuehn, R. E., and Liu, Z.: The CALIPSO Automated Aerosol Classification and Lidar Ratio Selection

650 Algorithm, J. Atmos. Ocean. Tech., 26, 1994–2014, https://doi.org/10.1175/2009JTECHA1231.1, 2009.

660

665

- Pappalardo, G., Amodeo, A., Apituley, A., Comeron, A., Freudenthaler, V., Linné, H., Ansmann, A., Bösenberg, J., D'Amico, G., Mattis, I., Mona, L., Wandinger, U., Amiridis, V., Alados-Arboledas, L., Nicolae, D., and Wiegner, M.: EARLINET: towards an advanced sustainable European aerosol lidar network, Atmos. Meas. Tech., 7, 2389–2409, https://doi.org/10.5194/amt-7-2389-2014, 2014.
- Peng, L., Yi, F., Liu, F., Yin, Z. and He, Y.: Optical properties of aerosol and cloud particles measured by a single-line-extracted pure rotational Raman lidar, Opt. Express, 29(14), 21947-21964. https://doi.org/10.1364/OE.427864, 2021.
 - Philip, S., Martin, R. V., Snider, G., Weagle, C. L., van Donkelaar, A., Brauer, M., Henze, D. K., Klimont, Z., Venkataraman, C., Guttikunda, S. K., and Zhang, Q.: Anthropogenic fugitive, combustion and industrial dust is a significant, underrepresented fine particulate matter source in global atmospheric models, Environ. Res. Lett., 12, 044018, https://doi.org/10.1088/1748-9326/aa65a4, 2017.
 - Ratcliffe, N. G., Ryder, C. L., Bellouin, N., Woodward, S., Jones, A., Johnson, B., Wieland, L.-M., Dollner, M., Gasteiger, J., and Weinzierl, B.: Long-range transport of coarse mineral dust: an evaluation of the Met Office Unified Model against aircraft observations, Atmos. Chem. Phys., 24, 12161–12181, https://doi.org/10.5194/acp-24-12161-2024, 2024.
 - Redemann, J., and Gao, L.: A machine learning paradigm for necessary observations to reduce uncertainties in aerosol climate forcing, Nat. Commun., 15, 8343, https://doi.org/10.1038/s41467-024-52747-y, 2024.
 - Rittmeister, F., Ansmann, A., Engelmann, R., Skupin, A., Baars, H., Kanitz, T., and Kinne, S.: Profiling of Saharan dust from the Caribbean to western Africa Part 1: Layering structures and optical properties from shipborne polarization/Raman lidar observations, Atmos. Chem. Phys., 17, 12963–12983, https://doi.org/10.5194/acp-17-12963-2017, 2017.
 - Rosenfeld, D.: Aerosol-cloud interactions control of Earth radiation and latent heat release budgets. In: Calisesi, Y., Bonnet, R.M., Gray, L., Langen, J., Lockwood, M. (eds) Solar Variability and Planetary Climates. Space Sciences Series of ISSI, vol 23. Springer, New York, NY. https://doi.org/10.1007/978-0-387-48341-2 12, 2006.
 - Rosenfeld, D., Andreae, M. O., Asmi, A., Chin, M., Leeuw, G., Donovan, D. P., Kahn, R., Kinne, S., Kivekäs, N., Kulmala, M., Lau, W., Schmidt, K. S., Suni, T., Wagner, T., Wild, M., and Quaas, J.: Global observations of aerosol-cloud-precipitation-climate interactions, Rev. Geophys., 52, 750–808, https://doi.org/10.1002/2013RG000441, 2014.
- Ryder, C. L., Highwood, E. J., Rosenberg, P. D., Trembath, J., Brooke, J. K., Bart, M., Dean, A., Crosier, J., Dorsey, J., Brindley, H., Banks, J., Marsham, J. H., McQuaid, J. B., Sodemann, H., and Washington, R.: Optical properties of Saharan dust aerosol and contribution from the coarse mode as measured during the Fennec 2011 aircraft campaign, Atmos. Chem. Phys., 13, 303–325, https://doi.org/10.5194/acp-13-303-2013, 2013.
- Ryder, C. L., Marenco, F., Brooke, J. K., Estelles, V., Cotton, R., Formenti, P., McQuaid, J. B., Price, H. C., Liu, D., Ausset,
 P., Rosenberg, P. D., Taylor, J. W., Choularton, T., Bower, K., Coe, H., Gallagher, M., Crosier, J., Lloyd, G., Highwood,
 E. J., and Murray, B. J.: Coarse-mode mineral dust size distributions, composition and optical properties from AER-D aircraft measurements over the tropical eastern Atlantic, Atmos. Chem. Phys., 18, 17225–17257, https://doi.org/10.5194/acp-18-17225-2018, 2018.
- Shen, H., Yin, Z., He, Y., Ansmann, A., Zhan, Y., Wang, L., and Jing, D.: Impact of Asian dust on cirrus formation over the central Pacific: CALIOP- and CloudSat-observation-based case studies, J. Geophys. Res. Atmos., 129, e2024JD041265, https://doi.org/10.1029/2024JD041265, 2024.
 - Shi, Y., Liu, X., Wu, M., Zhao, X., Ke, Z., and Brown, H.: Relative importance of high-latitude local and long-range-transported dust for Arctic ice-nucleating particles and impacts on Arctic mixed-phase clouds, Atmos. Chem. Phys., 22, 2909–2935, https://doi.org/10.5194/acp-22-2909-2022, 2022.
- 690 Shin, S.-K., Tesche, M., Kim, K., Kezoudi, M., Tatarov, B., Müller, D., and Noh, Y.: On the spectral depolarisation and lidar ratio of mineral dust provided in the AERONET version 3 inversion product, Atmos. Chem. Phys., 18, 12735–12746,

https://doi.org/10.5194/acp-18-12735-2018, 2018.

710

- Shin, S.-K., Tesche, M., Noh, Y., and Müller, D.: Aerosol-type classification based on AERONET version 3 inversion products, Atmos. Meas. Tech., 12, 3789–3803, https://doi.org/10.5194/amt-12-3789-2019, 2019.
- Shinozuka, Y., Clarke, A. D., Nenes, A., Jefferson, A., Wood, R., McNaughton, C. S., Ström, J., Tunved, P., Redemann, J., Thornhill, K. L., Moore, R. H., Lathem, T. L., Lin, J. J., and Yoon, Y. J.: The relationship between cloud condensation nuclei (CCN) concentration and light extinction of dried particles: indications of underlying aerosol processes and implications for satellite-based CCN estimates, Atmos. Chem. Phys., 15, 7585–7604, https://doi.org/10.5194/acp-15-7585-2015, 2015.
- Sinyuk, A., Holben, B. N., Eck, T. F., Giles, D. M., Slutsker, I., Korkin, S., Schafer, J. S., Smirnov, A., Sorokin, M., and Lyapustin, A.: The AERONET Version 3 aerosol retrieval algorithm, associated uncertainties and comparisons to Version 2, Atmos. Meas. Tech., 13, 3375–3411, https://doi.org/10.5194/amt-13-3375-2020, 2020.
 - Tan, I., Storelvmo, T., and Choi, Y.-S.: Spaceborne lidar observations of the ice-nucleating potential of dust, polluted dust, and smoke aerosols in mixed-phase clouds, J. Geophys. Res. Atmos., 119, 6653–6665, 2014.
- Tan, W., Zhao, G., Yu, Y., Li, C., Li, J., Kang, L., Zhu, T., and Zhao, C.: Method to retrieve cloud condensation nuclei number concentrations using lidar measurements, Atmos. Meas. Tech., 12, 3825–3839, https://doi.org/10.5194/amt-12-3825-2019, 2019.
 - Tesche, M., Ansmann, A., Müller, D., Althausen, D., Engelmann, R., Freudenthaler, V., and Groß, S.: Vertically resolved separation of dust and smoke over Cape Verde using multiwavelength Raman and polarization lidars during Saharan Mineral Dust Experiment 2008, J. Geophys. Res., 114, D13202, https://doi.org/10.1029/2009JD011862, 2009.
 - Tesche, M., Groß, S., Ansmann, A., Müller, D., Althausen, D., Freudenthaler, V., and Esselborn, M.: Profiling of Saharan dust and biomass-burning smoke with multiwavelength polarization Raman lidar at Cape Verde, Tellus B: Chem. Phys. Meteorol., 63, 649–676, https://doi.org/10.1111/j.1600-0889.2011.00548.x, 2011.
- Toledano, C., Torres, B., Velasco-Merino, C., Althausen, D., Groß, S., Wiegner, M., Weinzierl, B., Gasteiger, J., Ansmann,
 A., González, R., Mateos, D., Farrel, D., Müller, T., Haarig, M., and Cachorro, V. E.: Sun photometer retrievals of Saharan dust properties over Barbados during SALTRACE, Atmos. Chem. Phys., 19, 14571–14583, https://doi.org/10.5194/acp-19-14571-2019, 2019.
 - Ullrich, R., Hoose, C., Möhler, O., Niemand, M., Wagner, R., Höhler, K., Hiranuma, N., Saathoff, H., and Leisner, T.: A new ice nucleation active site parameterization for desert dust and soot, J. Atmos. Sci., 74, 699–717, https://doi.org/10.1175/JAS-D-16-0074.1, 2017.
 - Wang, T., Han, Y., Hua, W., Tang, J., Huang, J., Zhou, T., Huang, Z., Bi, J., and Xie, H.: Profiling dust mass concentration in Northwest China using a joint lidar and sun-photometer setting, Remote Sens., 13, 1099, https://doi.org/10.3390/rs13061099, 2021.
- Wehr, T., Kubota, T., Tzeremes, G., Wallace, K., Nakatsuka, H., Ohno, Y., Koopman, R., Rusli, S., Kikuchi, M., Eisinger, M.,
 Tanaka, T., Taga, M., Deghaye, P., Tomita, E., and Bernaerts, D.: The EarthCARE mission science and system overview,
 Atmos. Meas. Tech., 16, 3581–3608, https://doi.org/10.5194/amt-16-3581-2023, 2023.
 - Weinzierl, B., Petzold, A., Esselborn, M., Wirth, M., Rasp, K., Kandler, K., SchüTZ, L., Koepke, P., Fiebig, M.: Airborne measurements of dust layer properties, particle size distribution and mixing state of Saharan dust during SAMUM 2006, Tellus B: Chem. Phys. Meteorol., 61, 96–117, https://doi.org/10.1111/j.1600-0889.2008.00392.x, 2009.
- Weinzierl, B., Ansmann, A., Prospero, J. M., Althausen, D., Benker, N., Chouza, F., Dollner, M., Farrell, D., Fomba, W. K., Freudenthaler, V., Gasteiger, J., Groß, S., Haarig, M., Heinold, B., Kandler, K., Kristensen, T. B., Mayol-Bracero, O.L., Müller, T., Reitebuch, O., Sauer, D., Sch"afler, A., Schepanski, K., Spanu, A., Tegen, I., Toledano, C., Walser, A., Weinzierl, B., Ansmann, A., Prospero, J. M., Althausen, D., Benker, N., Chouza, F., Dollner, M., Farrell, D., Fomba, W.

K., Freudenthaler, V., Gasteiger, J., Groß, S., Haarig, M., Heinold, B., Kandler, K., Kristensen, T. B., Mayol-Bracero, O.
 L., Müller, T., Reitebuch, O., Sauer, D., Schäfler, A., Schepanski, K., Spanu, A., Tegen, I., Toledano, C., and Walser, A.:
 The Saharan aerosol long-range transport and aerosol–cloud-interaction experiment: overview and selected highlights,
 Bull. Am. Meteorol. Soc., 98, 1427–1451, https://doi.org/10.1175/BAMSD-15-00142.1, 2017.

740

- Winker, D. M., Vaughan, M. A., Omar, A., Hu, Y., Powell, K. A., Liu, Z., Hunt, W. H., and Young, S. A.: Overview of the CALIPSO Mission and CALIOP Data Processing Algorithms, J. Atmos. Ocean. Tech., 26, 2310–2323, https://doi.org/10.1175/2009JTECHA1281.1, 2009.
- Zhao, B., Wang, Y., Gu, Y., Liou, K.-N., Jiang, J. H., Fan, J., Liu, X., Huang, L., and Yung, Y. L.: Ice nucleation by aerosols from anthropogenic pollution, Nat. Geosci., 12, 602–607, https://doi.org/10.1038/s41561-019-0389-4, 2019.
- Zhou, Z., Ma, Y., Yin, Z., Hu, Q., Veselovskii, I., Müller, D., and Gong, W.: A modified look-up table based algorithm with a self-posed scheme for fine-mode aerosol microphysical properties inversion by multi-wavelength lidar, Remote Sens., 16, 2265, https://doi.org/10.3390/rs16132265, 2024.